780

co-spokesman: Ronald Lipton
412-268-3887
BITNET: LIPTON@CMPHYS
Douglas Potter
412-268-2728
BITNET: POTTER@CMPHYS
Physics Department
Carnegie-Mellon University
Pittsburgh, Pa. 15213

PROPOSAL TO STUDY CHARM PRODUCED BY 850 GEV PROTONS

J. Volk, J. Wilcox, P. Yager
Physics Department, University of California, Davis, California

R.M. Edelstein, D. Gibaut, R. Lipton, D. Potter, J. Russ
Physics Department, Carnegie-Mellon University, Pittsburgh, Pennsylvania

S. Fredricksen, B. Lundberg, N. Reay, K. Reibel, R. Sidwell, N. Stanton
Department of Physics, Ohio State University, Columbus, Ohio

G. Kalbfleisch, P. Skubic, J. Snow, S. Willis
Department of Physics and Astronomy, University of Oklahoma, Norman, Oklahoma

March, 1987

SUMMARY OF THE EXPERIMENT

We propose an experiment to study the properties of charm particles produced in hadronic interactions with a machine energy proton beam. The principal goals of the experiment are to study lifetimes and spectroscopy of charm baryons, to explore production dynamics and correlations, and to search for coherent diffractive production of charm off silicon. The data sample will include an estimated 1000 reconstructed Λ_c's to the p K π mode alone and a total of 50,000 reconstructed D's to many modes. Twenty percent of the charm particles will be in 5,000 events in which both decays are reconstructed.

The experiment will be carried out with our existing E653 hybrid emulsion spectrometer. Major components of the spectrometer are a vertex detector unique for its precision, redundancy, and large aperture, 12 multi-hit "vector" drift chambers, highly segmented electromagnetic and hadronic calorimetry, and an independent muon spectrometer. The only major modification to the apparatus will be to replace the nuclear emulsion target with an active electronic target and a "multiplicity jump trigger". Decays of pairs of charm particles are detected by an increase in the multiplicity of charged particles in an evacuated decay region downstream of the target. Multiplicity is measured by pulse heights in silicon detectors bracketing the decay region. A trigger is generated if the difference in pulse height between the downstream and upstream dectectors corresponds to three or more minimum ionizing particles. The trigger has the properties that its efficiency is correlated with spectrometer acceptance and that it selects events in which each charm decays into a multiprong mode well downstream of the target. These properties result in a data sample in which two vertices can frequently be reconstructed; thus, not only is the fraction of events containing two reconstructed charm particles large, but clean topological handles can be used to reduce background for events in which only one charm particle can be reconstructed.

We intend to begin running the proposed experiment upon the completion of our E653 emulsion exposure, near the end of the third (1988) Tevatron II running cycle, and to finish in the fourth cycle. The multiplicity jump trigger will be tested parasitically during the 1987 run of E653. Because little new apparatus or software is required, experimental setup can be done quickly and analysis can be done efficiently.

Table of Contents

1. INTRODUCTION

After over a decade of intense experimental effort the study of hadronic production of charm is now becoming a mature field. Experimental breakthroughs have been made in the deployment of high resolution detectors such as silicon microstrip detectors, nuclear emulsions, and high resolution bubble chambers. New detector technologies have been complemented by improvements in data acquisition systems which allow experiments to record an order of magnitude more data per run. As experimental technique becomes more refined the questions experiments are designed to answer can become more focussed. Experiments can now be designed to explore specific problems in hadronic charm production.

The major objectives of this experiment are the following:

1. To measure charmed baryon production, spectroscopy, and lifetimes.

2. To investigate correlations and production dynamics of charm particles.

3. To search for diffractive production of charm.

These goals will be addressed with a sample of reconstructed decays including 1000 Λ_c's to the p K^- π^+ mode alone and 50,000 D's to many modes. Twenty percent of the D's, (5,000 pairs) will have both charm particles reconstructed.

Our proposed experiment will use the existing E653 spectrometer in an all-electronic configuration. The nuclear emulsion target will be replaced with an active electronic target and a multiplicity jump trigger, which will permit triggering inclusively on the decays of pairs of charm particles. Because a primary goal of this experiment is to explore charm baryon physics, it will be run with a machine energy proton beam. We intend to begin the experiment after the completion of the E653 emulsion runs approximately one month before the end of the third (1988) Tevatron II running cycle, and to complete it in the following cycle. The experiment requires little new hardware or software, so neither experimental setup nor offline analysis will require long preparation.

The ability to detect secondary vertices with good efficiency and with little background is crucial for the success of any heavy quark experiment. Measurements along track trajectories must be both precise and redundant. The E653 spectrometer has 18 planes of silicon strip vertex detectors with analog readout and 12 multi-hit "vector drift"

chambers. These features, together with its highly seqmented calorimetry, provide the E653 spectrometer with unexcelled capability for identification of charm events and complete reconstruction of the entire topology. As in E653, charm candidate events will be identified by secondary vertices and tracks with large impact parameters rather than by peaks in mass spectra. At a later stage in the analysis each charm candidate will be fit to a specific decay hypothesis. Thus, the experiment suffers no biases introduced by the selection of specific decay modes

2. PHYSICS MOTIVATION AND GOALS

Our understanding of the physics of hadronic charm production dynamics is still incomplete. Currently, the best production data come from the LEBC (NA27[1] AND NA16[2]) hybrid bubble chamber experiments. The 360 GeV pion data from NA27 show a two component x_F distribution. D's having no quark in common with the pion are produced centrally with a a $(1-x_F)^7$ distribution. Those which share a quark with the pion are produced with a forward, $(1-x_F)^1$, distribution. The gluon fusion model seems to describe the central piece of the cross section quite well, but the forward region is not on as firm a footing. According to the Lund model[3] the forward component of charm production is due to a color interaction between the projectile fragment and the charm quark, which accelerates the latter.

An open question is whether the x_F distribution for D's which have a quark in common with the proton is different from that for D's which do not. Also unknown is whether Λ_c production in a proton beam will exhibit the same leading particle effect observed in hyperon production by protons[4, 5] and in Ξ_c production by a Σ^- beam[6]. NA27 data for charm produced in a proton beam show no leading particle effects for any species of charm particles[7], while ISR data for Λ_c's appear to have the leading behavior[7]. The Lund model predicts that the x_F distribution of Λ_c's will have a flat component and that the Λ_c's will saturate charm production at large x_F. See Figs. 1 and 2.

Events in which both charm particles are reconstructed provide the maximum possible information about the underlying production dynamics. These events permit the most detailed tests of model predictions, such as charm species correlations and kinematic correlations in x_F and P_T. The current status is that statistics are poor and correlations are not understood. Data from NA27[8] are consistent with no kinematic correlations beyond

those imposed by phase space, although agreement with other models seems acceptable. Better statistics over a wide range of kinematic variables are needed.

Pairs of charm particles may also be produced by diffractive mechanisms. The intrinsic charm model predicts that the proton will contain as a piece of its wave function the state $|uudcc\rangle$[9, 10]. Brodsky, et al.[9] estimate the amount intrinsic charm to be 0.3%, which would imply that diffraction could account for a few percent of the total charm production cross section. The notion has the precedent that N* resonances on low lying Regge trajectories frequently have substantial branching ratios to strange particles[11]. This model predicts diffractive production by dissociation. 'QCD Pomeron' models[12, 13, 14] treat the Pomeron as a multi-gluon state. In these models a hadron-Pomeron collision is much the same as a hadron-hadron collision if the center of mass is taken to be that of the colliding particles. Diffractive production of charm can occur by creating the charm quarks. The two classes of models can be distinguished by their different thresholds kinematics[15]. Diffraction via intrinsic charm turns on sufficiently rapidly above threshold that the process can occur coherently off nuclei (see Appendix II.). Diffraction via the 'QCD Pomeron' turns on slowly above threshold, as in hadron-hadron reactions[14]. Coherent diffractive production of charm off nuclei is unlikely in these models because momentum transfer to the nucleus must be large.

It is important that a search for coherent diffractive production of charm be carried out at the highest possible energy and preferrably off a light nucleus. For large diffractive masses the (momentum transfer)^2 to the nucleus, $t_{min'}$ varies as M^4/p^2, where M is the mass of the diffractively produced state and p is the beam momentum. In order that the reaction be coherent, the momentum transfer to the nucleus must be less than $1/r$, where r is nuclear radius. Therefore, the maximum invariant mass that can be produced diffractively[16] varies as $p^{1/2}/A^{1/6}$; it is 13 GeV/c^2 for 850 GeV/c protons on silicon. Since the threshold mass for producing charm is 4 GeV/c^2, use of beam energies much lower than 850 GeV/c will severely limit the phase space available and may not accomodate kinematic threshold effects. No searches for coherent diffractive production of charm have been reported, and the data that do exist do not appear to have been collected at sufficiently high energy with a vertex detector having the precision to resolve the topology.

Diffractive production of charm is not only interesting as a new phenomenon, but if it exists, could provide the basis of a powerful experimental technique. Charm pairs would be produced in low multiplicity events and carry most of the beam momentum. Such events could be both detected and analyzed with high efficiency. Diffractive production in a baryon beam could be a rich souce of charm baryons.

The field of charm baryon physics is virtually open. Typical data samples are either very small, or contain significant background contamination. The Λ_c lifetime will soon be measured to 10-15%, which is five times worse than the precision anticipated for D lifetimes[17]. Fig. 3 shows the lower lying charm baryon levels and identifies those which have been observed. Only the neutral and doubly charged states of the Σ_c have been observed[11, 18]. None of the spin 3/2 or other excited states has been seen. Only one charm-strange baryon, the Ξ_c^+, has been observed[6, 19]. Fig. 3 shows that good photon and π^0 detection is required to see many of the excited baryons.

The primary goals of the experiment are the following:

1. Study charm baryon physics. The Λ_c is the key to studies of non-strange charm baryons, since all are expected to decay to it. We expect to collect 1000 reconstructed Λ_c decays to the p K π mode alone, as well as a substantial number to other modes. The sample will be used to measure the Λ_c lifetime to better than 5%, look for the Σ_c^+ and measure mass splittings between the Σ_c's, look for the spin 3/2 and other excited states, and study production dynamics for all observed charm baryons. The $\Sigma_c \dashrightarrow \Lambda_c \pi$ cascade decays are particularly attractive from an experimental point of view because they provide the same handle on baryons as the D* cascade decay does on mesons. Both the neutral and doubly charged Σ_c's have signatures which cannot be confused with D*'s. We estimate a yield of 200 Ξ^+_c's (which would permit a 10% lifetime measurement) and will look for other charm baryons containing one or more strange quarks.

2. Study kinematic distributions of charm particles. With our expected sample of 50,000 reconstructed D's we will be able to map out x_F and P_T distributions with high statistics. The important objectives are to measure their dependence on charm species and to extend current measurements closer to kinematic boundaries. Differences in x_F dependences can be measured most effectively at large x_F, where our trigger is most efficient.

3. Study production correlations of charm particles. Twenty percent of our sample will be events in which both charm particles are reconstructed. These

5000 pairs will be used to study x_F, P_T, and species correlations and search for incoherent diffractive production. The large sample will allow details of correlations to be studied in sparsely populated regions of phase space, such as at high P_T, and permit correlations in one variable to be studied as a function of another.

4. Search for coherent diffractive production of charm off silicon. If the prediction that the proton contains 0.3% intrinsic charm is correct, 5% of the total charm cross section is diffractive and we would collect in a 2 week run 4000 D's and 800 Λ_c's to the p K^- π^+ mode alone. Thus, the experiment is sensitive to an intrinsic charm component of the proton at the level of 3 x 10^{-5}.

3. EXPERIMENTAL TECHNIQUE

The outstanding success of E691[17] depends in part on the 1% charm-to-background ratio inherent in photoproduction. Had the experiment been run with no modifications other than the use of a hadron beam (with a 0.1% charm-to-background ratio), mass peaks in most decay modes would have been barely visible. This and the fact that the yield resulting from years of effort by the NA11 group is comparable in statistics[20] to that of LEBC lead one to the conclusion that charm hadroproduction is still a difficult field. The success of LEBC and other visual techniques demonstrates the importance of a high density of precise information, and thus defines a model for non-visual techniques.

As in our hybrid emulsion experiment, E653, we will identify charm events in the proposed experiment solely on the basis of topology, and later fit individual decays to a specific hypothesis. When compared to selecting charm on the basis of peaks in mass spectra, this method has the advantage that no bias is introduced by the selection of specific decay modes, so, for example, beauty events would not be rejected. However, in order for the approach to work well, it is important that the events to be selected have clear topological handles, that the charm-to-background ratio be optimized at the trigger level, and that the probability of pattern recognition errors, such as fake track and vertices, be small. According to the model defined above, the latter requirement means that the vertex detector should have very high precision and redundancy.

The existing E653 spectrometer (Figs. 4 and 5) has such a vertex detector, which is unique for its large aperture, as well as for its precision and redundancy. In the proposed

experiment we will exploit the spectrometer but replace the nuclear emulsion with an active electronic target and a multiplicity jump trigger. The spectrometer will be used without major modifications, and is described in a later section.

The basic idea behind the multiplicity jump trigger is to detect the decays of a pair of charm particles by observing a multiplicity increase of three or more in an evacuated decay region downstream of a production target. Fig. 6 illustrates the principle schematically. Pulse heights in silicon detectors bracketing the decay region are used to measure the multiplicity change. To minimize the effects of Landau fluctuations on the trigger efficiency and rate the maximum number of particles entering the decay region is required to be less than 9.

In the proposed experiment the charm-to-background ratio is optimized in several different ways. Use of an 850 GeV/c beam maximizes the charm cross section for a fixed target experiment, minimizes the effects of multiple scattering on vertex finding, and insures the longest possible flight path length of the decaying particles. Other important factors are related to the multiplicity jump trigger and the interplay between it, the beam energy, and the vertex detector. As discussed in the following paragraphs, the trigger selects a sample of charm which is easier to analyze and has less background than typical charm events.

1. Data from LEBC[21] show that the distribution of charged multiplicity accompanying charm particles is very broad, so that the upper limit of 9 particles entering the decay region retains a substantial fraction of the charm events. In preliminary 800 GeV proton data from E743[21] roughly 50% of the background and more than 20% of the charm survive the upper limit cut. (In the 400 GeV proton data from NA27, which has an order of magnitude better statistics, 40% of the charm survives, so use of the E743 result appears conservative.) The upper level cut alone does not improve the ratio of charm-to-background events. However, in addition to making it possible to implement an effective multiplicity jump trigger, the cut forces the average number of primary tracks to be 6 or 7. The low multiplicity has many advantages, including a small probability per event of having a secondary interaction ($<1.5\%$) and a reduction of the number of ambiguous assignments of tracks to vertices, the number of fake vertices, and the amount of combinatoric background. The latter consideration is particularly important for studies of excited charm baryon states.

2. The trigger efficiency for the sample of charm in which each decays in the

decay region to two or more stable charged particles is 50%. For this sample the net trigger efficiency, which includes a factor of .2 for the probability to survive the upper level cut, is 10%. The trigger efficiency for the 50% of the background events which survive the cut is 2%. Thus, the net improvement in the charm-to-background ratio is more than 10 for the sample.

3. Because charm particles must reach the decay region to generate a trigger and are more likely to do so at large x_F, spectrometer efficiency is correlated with trigger efficiency. Fig. 7 shows the probability that a Λ_c --> p K^- π^+ decay be accepted by the spectrometer as a function of x_F. Fig. 8 shows the joint probabilty that the same decay both reach the decay region and be accepted by the spectrometer. Comparison of the two plots demonstrates the correlation. Average acceptance for decays occuring in the decay region varies from 97% for a Λ_c to 78% for a charged D.

4. In order for the trigger to be efficient, both charm particles must reach the decay region. This requirement has three advantageous side effects. The first is that production and decay vertices are unlikely to merge; such merging has the consequence that the position of the production vertex is incorrectly predicted. (The active target also helps to define the production vertex.) The second is that the fraction of events in which both charm particles in the pair are accepted and reconstructed is enhanced. The third is that decay vertices of unreconstructed charm particles can be used to purify the sample of fully reconstructed partners. The geometrical acceptance for at least two charged tracks from a charm decay vertex is 85%, and is greater if only a single prong is required. Large vertex detector aperture (+/- 139 mr.), high beam energy and the positive correlation between geometrical acceptance and trigger efficiency are responsible for the last two properties.

5. The trigger is inefficient for 1 prong ('kinks') and 0 prong decays. Because these decays cannot usually be analyzed, their loss is not important. The trigger is also inefficient for decays which occur before the decay region. The loss of these events is similarly not important. Background for this class of events would be larger both because the decays occur in material and also because the decays would frequently be too close to the interaction vertex to permit unambiguous identification. Thus, most of the events for which the trigger is inefficient are those which would be eliminated in offline analysis.

The ACCMOR collaboration evaluated a similar multiplicity jump trigger in NA32 and, despite the fact that the technique worked, decided not to use it[22]. Reasons for not using it were that the reduction in background trigger rate was a factor of 2 to 3 less than

anticipated, that online calibration and stability were problems, and that the trigger could bias the data. The multiplicity jump trigger to be used for the proposed experiment differs in that it is much simpler, that the decays are forced to occur in vacuum to eliminate background from secondary interactions, that an upper level cut on the number of primary particles is made to reduce Landau fluctuations, and that the system is less sensitive to alignment. We have extensive experience with the electronics to be used for the trigger (identical preamps are used on our liquid argon calorimeter) and have had no problems with stability. Finally, it is true that the trigger biasses the data, as does any trigger. The positive aspects to the bias have been discussed; the negative aspects are addressed later.

3.1. IMPLEMENTATION

During the 1985 run of E653 we evaluated a prototype multiplicity jump trigger. Results from that test, which are described in Appendix I., were used to design the devices to be used for this experiment and to predict their performance. During the 1987 run of E653 we will collect data parasitically in order to optimize the design of the trigger. Data will be obtained with the detectors and preamplifiers to be used in the proposed multiplicity jump trigger, and will be recorded with ADC's.

Fig. 9 is a schematic of the multiplicity jump trigger which we will use for most of the proposed experiment. It consists of the following components:

1. The beam silicon strip detector (SSD), which has 100 micron pitch. 50 strips will be instrumented.

2. The uptream interaction veto counter, which is a 300 micron thick silicon wafer detector.

3. The active target. The target consists of 6 alternating layers of 500 micron thick synthetic diamond and 300 micron thick silicon wafer detector. Its mass is .735 g/cm^2, 71% of which is carbon. The total target length is 2.4 mm.

4. The upstream multiplicity detector. This is a 100 micron pitch 200 micron thick SSD identical to the beam SSD. It is placed 400 microns downstream of the end of the target, so the mean distance between the interaction vertex and the beginning of the decay region is 1.8 mm. 80 strips will be instrumented.

5. The 6 cm. long evacuated decay region.

6. The two downstream multiplicity detectors. These are 1 mm. pitch SSD's. 37 strips on each detector will be instrumented.

The trigger is organized as a two level system. Level one requires an interaction in the target, and is implemented in commercial fast logic. Level two is implemented in non-standard modules, in which sequential operations are synchronized by a clock started by the level one trigger. The level two trigger accomplishes the following:

1. Events in which two or more particles would enter the target are eliminated by the upstream interaction veto counter.

2. x and z coordinates of the interaction vertex are determined from hits in the beam SSD and pulse height in the active target detectors, respectively.

3. A +/- 300 mr. angle from the interaction vertex is defined in the x - z plane at the upstream multiplicity detector. Pulse heights of strips within the angle are summed to form the 'before' pulse height.

4. Pulse heights for all strips in each of the two downstream multiplicity detectors are summed. The smaller of the two is used as the 'after' pulse height to minimize fluctuations.

5. The 'before' pulse height is subtracted from the 'after'. This is the multiplicity jump.

6. A trigger results if the multiplicity jump exceeds 3 (in units of minimum ionizing particles) and if the 'before' pulse height is less than 9. The latter requirement serves to limit the number of particles entering the decay region.

Electronics used for level two of the multiplicity jump trigger are conventional. For every interaction pulse heights from all wafers and strips are stored in integrate-and-hold circuits. Thus, arithmetic operations can be carried out at low bandwidth. The indices of the strip hit in the beam SSD and the first target wafer downstream of the interaction are encoded into an address for a RAM, which is programmed with the acceptance angle and strip offset. Output bits of the RAM are used to gate the integrate-and-hold's for the upstream SSD to a summing amplifier. Final arithmetic operations are done with comparators. Because the RAM is programmable, there is considerable flexibility for making software changes in acceptance as well as alignment. All pulse heights will be digitized for use in offline anlaysis. The total number of instrumented channels is 209.

The design is driven primarily by the requirement that the effects of spallation protons from the primary interaction be minimized. Diamond was chosen as the target material for its low atomic number (and, consequently, small average number of spallation protons) and its high density, 3.5 g/cm^3. We calculate from published data[23] that in about 20% of the interactions a spallation proton will be within +/− 300 mr. of the beam, and thus contribute to to the 'before' pulse height.

3.2. BIASES IN THE TECHNIQUE

As all electronic experiments, the proposed experiment has several biases. Two are due to the fact that the target material is not hydrogen. Measured distributions of kinematic variables and normalization may have a complex A dependence[7]. However, the important objectives are to compare the distributions for different species of charm particles and to investigate correlations. Nuclear effects are unlikely to bias these results.

A second nuclear effect is an inefficiency caused by spallation protons from the primary interaction. Because of its low energy a spallation proton can deposit a very large energy in the multiplicity detector upstream of the decay region, and thereby ruin the multiplicity measurement. The effect is calculated to reject 20% of the events (see Appendix I.), and can be compensated by running the experiment with an interaction trigger for a few hours.

The multiplicity jump trigger biases the results in two ways also. The first, the requirement that both charm particles reach the decay region, is similar to the effects of geometrical acceptance and can be corrected by similar techniques. All estimates of yields are based on the assumption that there are no correlations in x_F, which is consistent with the LEBC result[21]

The second is similar to the nuclear effects and potentially more serious. If the distributions of kinematic variables for charm particles depend significantly on charged multiplicity, a bias may be introduced by the cut which requires that no more than nine particles enter the decay region. Effects of the cut can be compensated by collecting some data with the cut level raised and determining how measured x_F and P_T distributions vary with the multiplicity of charged particles and π^0's accompanying the charm pairs.

3.3. IMPLEMENTATION FOR COHERERENT PRODUCTION

The multiplicity jump trigger used for the search for coherent diffractive production of charm is tailored to the specific characteristics of the process. In a coherent process no spallation protons can be produced and the average number of charged particles accompanying the charm is quite small[16]. Thus, the only signature of an interaction can be nuclear recoil energy. The charm particles are produced on the average with half the beam momentum each. Therefore, to measure the nuclear recoil energy and detect the interaction vertex the target must be 100% active, and to contain the charm particles the decay region must be quite long. Because spallation protons do not cause experimental problems, silicon strip detectors need not be used in the trigger. Silicon wafer detectors are adequate, and thus, a simple multiplicity jump trigger seems ideally suited to this measurement.

The multiplicity jump trigger for coherent production consists of the following components:

1. The target assembly, which consists of twenty 300 micron thick silicon wafer detectors spaced on 400 micron centers. The first wafer in the stack serves as an upstream interaction veto counter. The last two comprise the 'before' multiplicity detectors. The 17 wafers in between are the active target. (A similar target was used in an early experiment on diffractive dissociation[24])

2. A 15 cm. long decay region.

3. Two 'after' silicon wafer detectors

The trigger, also organized as a two level system, works as follows:

1. Events in which 2 or more particles would enter the target are eliminated by the upstream veto counter.

2. The wafer with the minimum pulse height in the 'before' pair is used for the 'before' multiplicity measurement.

3. The wafer with the minimum pulse height in the 'after' pair is used for the 'after' multiplicty measurement.

4. The multiplicity jump is defined as the 'after' – 'before' pulse height difference.

5. A trigger results if the multiplicity jump corresponds to between 3 and 10 particles and if the 'before' pulse height corresponds to 6 or fewer particles.

To avoid biasing the data no information from the target will be used in the trigger. In offline analysis pulse height information from the active target will be used to discriminate against nuclear breakup and to measure nuclear recoil energy.

4. THE E653 SPECTROMETER

Major components of the E653 spectrometer (Figs. 4 and 5) are beam detectors, a silicon strip vertex detector, a charged particle spectrometer (consisting of the vertex detector, a magnet, and a set of "vector" drift chambers), a time-of-flight hodoscope, an electomagnetic calorimeter, a hadron calorimeter, and an independent muon spectrometer. Components of the spectrometer most important for the success of the proposed experiment and unique to it are the 18 plane high precision vertex detector and the 3400 channel electromagnetic calorimeter; each of these devices has a very large (+/- 140 mr.) aperture. By emphasizing precision and redundancy the single magnet design provides good momentum resolution in a short spectrometer and does not compromise photon detection.

General characteristics of the spectometer are as follows. Momentum resolution is 0.7% RMS below 55 GeV in the multiple scattering limit and (0.017 x p)% at higher momenta. This leads to the mass resolution shown in Fig. 10. Acceptance for $x_F > 0$ (see Fig. 7) is above 90% for decays to all charged particles. K_s's and Λ's can be reconstructed if the decays occur in the meter between the production target and the midplane of the analysis magnet; Fig. 11 shows neutral "V" detection efficiency.

The following subsections describe the various systems comprising the spectrometer to be used for the proposed experiment and the modifications to the E653 apparatus required. for the proposed experiment. Because we feel that a well understood spectrometer with existing software has signifcant advantages for timely running and analysis, we plan no major changes to the existing apparatus.

4.1. BEAM AND BEAM SYSTEM

The proposed experiment uses the existing NE beamline, which is capable of transporting the machine energy protons required for this experiment. Beam particles are measured by two stations of silicon strip detectors (SSD's). Each station consists of six detectors arranged in three 60 degree views. The detectors are 20 micron pitch and are read out every 60 microns with the coordinate calculated using capacitive charge division. The anticipated resolution for beam particles projected to the target is 5 microns RMS.

The required modifications of the existing beam measuring system are to replace a drift chamber with SSD's and to reconfigure the existing SSD's.

4.2. VERTEX DETECTOR

The vertex detector to be used for the proposed experiment is unique for its large aperture, for its redundancy, and for its precision. It consists of 18 planes of silicon strip detectors arranged in three 60 degree views with 6 detectors per view. See Fig. 4. The detectors are mounted in a 27 cm long package immediately downstream of the target assembly. All SSD's are 300 microns thick; all but the first three have strips on 50 micron centers; and all use capacitive charge division to reduce (to 10,000) the number of channels digitized by ADC's. The first three detectors are 3 x 3 cm. in active area and have 12.5 micron pitch in the central 6 mm. where alternate strips are read out. The next nine detectors are 5 cm. square and in the central 8 mm. every strip is read out; the last six SSD's are 9.6 cm. square and in the central 25.6 mm. every strip is read out.

Data acquired during the first run of E653 in 1985 (in which eighteen 5 cm. x 5 cm. detectors were used) provide several measures of the vertex detector performance. In the central region the system had 8.5 micron RMS resolution per plane (see Fig. 12) . At the periphery, where readout is on every fifth strip, the resolution was 22 microns. Using the beam track along with those from the interaction, we measured the RMS resolution at the primary vertex to be 7 microns in x and y and 360 microns in z. In the proposed experiment the resolution will improve to 4 microns in x and y and to 200 microns in z. A stringent test of both apparatus and software is a comparison of the projected impact parameter distribution of high momentum tracks with a similar distribution obtained for non-interacting beam tracks (see Fig. 13). Note that the two distributions have similar widths despite the fact that the tracks used for the impact parameter distribution

are in the busiest region of the vertex detector.

The vertex detector for the proposed experiment is the same as that to be used in the second run of E653 (which is similarly unique), except that the last three midsized SSD's must be replaced with 9.6 cm. square SSD's.

4.3. SPECTROMETER DRIFT CHAMBERS

The drift chamber system downstream of the SCM104 magnet consists of 12 planes of 1.7 meter square "vector" drift chambers. Each chamber measures a track 5 times in z, providing a "mini-vector" with an angular resolution of 5mr. Large angle tracks can be adequately reconstructed using hits in only three of the chambers. Drift chamber data are recorded with Lecroy 1879 multi-hit fastbus TDC's, which digitize both the leading and the trailing edge of the sense wire pulses. Because the spread in the pulse widths is small, a hit position can be determined by the trailing edge of the pulse as well as by the leading edge. Consequently, hits can be resolved even when their sense wire pulses overlap, and the resulting double hit resolution is 600 microns. It is not unusual to reconstruct 5 tracks in the central cell alone. Position resolution of a single wire is 110 microns RMS for beam tracks and 140 microns in high multiplicity proton-emulsion interactions.

The spectrometer drift chamber system was designed to operate at low beam intensities. For the proposed experiment we will improve by an order of magnitude the rate capability of the system with more sensitive preamplifiers on the central drift cells.

4.4. CALORIMETRY

The calorimetry was designed to accomodate high multiplicity events in which showers frequently overlap. To detect electromagnetic showers we use a 1.8 meter square lead-liquid argon calorimeter segmented into three sections in depth. The readout is organized into x and y projective strips to provide good position resolution, and a set of pads to match the two projections. This system routinely reconstructs 15 shower events. The two shower resolution is less than 1 cm and the position resolution is better than 1 mm. The central 6.4"x6.4" square is further subdivided into 256 rectangular pads in each view. Fig. 14 shows the resolution ($12.5\%/E^{1/2} + 2.5\%$, RMS) of the calorimeter for 10 GeV electron showers. Fig. 15 shows the di-photon mass resolution in the π^0 mass region. Both figures are based on a preliminary analysis.

Hadron calorimetery is provided by an iron-proportional tube calorimeter. This device has 16 samples separated by 2" of steel and is also read out using a strip-pad geometery.

No modifications of the present calorimetry are required for the proposed experiment.

4.5. MUON SYSTEM

Muon identification uses an independent muon spectrometer. Muon tracks are measured by 12 planes of 3 meter square drift chambers - 6 each upstream and downstream of a toroid magnet. The upstream chambers follow the hadron calorimetery and 30 centimeters of iron absorber. The toroid is 1.34 meters thick and provides a P_T kick of .8 GeV/c. The downstream muon chambers are followed by an additional 1.5 meters of absorber and two walls of scintillation counters. The muon momentum required to penetrate the system is 7 GeV.

No modification of the present muon system is required for the proposed experiment.

4.6. HADRON IDENTIFICATION

Our hadron identifier is a wall of time-of-flight counters immediately downstream of the spectrometer drift chamber system. These can separate protons from pions up to 7 GeV/c and kaons from pions up to 3.5 GeV/c.

No modification of the time-of-flight system is required for the proposed experiment.

4.7. DATA ACQUISITION

E653 was the first experiment to use a full commercial fastbus system. Fastbus is well matched to the high density of information provided by the spectometer. We have a total of 16,000 ADC channels and 2200 channels of multihit TDCs. An average event contains 26,000 bytes of data. Our fastbus is organized as a 12 crate system, 11 data acquisition crates and a master crate containing Lecroy 1891 buffer memories. All data collected during the spill are stored in these buffer memories and then transferred to a VAX 750 for tape writing. A MicroVax is used to monitor apparatus. We will be able to record 600 events in a 20 second spill.

To accomodate the vertex detector upgrade for the proposed experiment we will need two more fastbus crates with the necessary interfacing and control modules and some additional ADC's.

4.8. EVENT DISPLAYS

Event displays from the 1985 nuclear emulsion run of E653 provide a qualitative 'feel' for detector and software performance. Typical event topology for the proposed experiment should be simpler than the events shown, not only because the target is thin and composed of light nuclei but also because the maximum number of primary tracks must be less than 9. Figs. 16, 17, and 18 are event displays for the vertex detector, the spectrometer drift chamber system, and the liquid argon calorimeter, respectively. Figs. 16 and 17 are for a charm candidate. Note that in the first two systems the density of information is sufficiently high that tracks do not have to be reconstructed to be seen. As in visual techniques the pattern is apparent from the hits.

5. YIELDS AND RATES

5.1. YIELDS AND RATES FOR NON-DIFFRACTIVE CHARM

1. **BEAM:** We plan to run the experiment with a 0.35 MHz machine energy (850 GeV/c) proton beam. We assume for a 16 week run 16×10^5 seconds of protons on target, which corresponds to 83 hours of beam time per week.

2. **TARGET:** The target, described in section 3, is .735 g/cm^2 and 0.81% of an absorption length. The interaction rate is 2.8 kHz. The total number of interactions is 4.48×10^9.

3. **CROSS SECTION:** To estimate yields we use the E743 result that the cross section for D pair production by 800 GeV/c protons is 30 microbarns[25], and assume a linear A dependence. (The A dependence used here is that which seems to give agreement between the data on hydrogen and those on light nuclei[7].) The probability per interaction of producing D pairs is .0016.

4. **TRIGGER ACCEPTANCE:** To benchmark the experiment in a transparent way we will consider first only pairs of neutral D's. The LEBC data[26] show that neutral D's outnumber charged by a factor of 2. If pairing is statistical, one expects the following ratios for pairs of D's: neutral–neutral:neutral–charged:charged–charged = 4:4:1. Thus 4/9's of all D pair events should contain two neutral D's. The trigger acceptance depends on the following

factors:

a. We require both D's of the pair to decay to two or more prongs. 86% of neutral D decays are to two or more prongs[27], so the experiment accesses 74% of all neutral D pairs produced.

b. The upper limit on the number of charged particles entering the decay region is 9. From preliminary E743 data[21] we find that more than 20% of the total charm produced is in this sample, as is about 50% of the background.

c. Of the events which pass the upper limit cut, 50% of the neutral D pairs will survive the requirement that the multiplicity jump be 3 or greater as will about 2% of the background. The efficiency was calculated for multiplicity increase of 4 in the decay region. Every charm pair in the sample must have an increase at least that large.

d. The probability that both neutral D's get to the decay region is .26 for central production.

5. **D YIELD:** The net yield of neutral D pairs is
$.0016 \times 4/9 \times .74 \times .2 \times .5 \times .26 = 1.37 \times 10^{-5}$/interaction,
for a total of 61,000. Adding the charged-neutral and charged-charged pairs gives a total of 112,000 D pairs on tape. See Table I.

6. **Λ_c YIELD:** The Λ_c yield is calculated in a similar way. The input consists of the following:

a. We use as a benchmark the p K^- π^+ mode, for which the branching ratio was estimated by the Mark II group[28] to be 2.2%. (There are many other modes which could be detected, albeit with lower efficiency. The p K^- π^+ π^0 and Σ^- π^+ π^+ modes, for example, have branching ratios estimated theoretically to be 3% and 6%, respectively[29], which are to be compared to the 5% estimate for the p K^- π^+ mode. Because the estimated cross section depends on the Mark II p K^- π^+ branching ratio, other modes are ignored in the yield calculation.)

b. The Λ_c is paired twice as frequently with a neutral D as with a charged, so 2/3's of all Λ_c's are accompanied by a neutral D.

c. The mean life of the Λ_c is .23 ps[11]. We assume that the Λ_c is produced with the distribution $dN/dx_F = (1-x_F)^n$. The probability that the Λ_c get to the decay region is .40, independent of n for $2 < n < 7$. The probability that a Λ_c-neutral D pair get to the decay region is .20,

TABLE I - CHARM YIELDS

	D^oD^o	D^oD^++c.c.	D^+D^-	$\Lambda_c D^o + \Lambda_c D^- + c.c.$
Produced pairs	3.2×10^6	3.2×10^6	8×10^5	4.8×10^6
Net branching fraction for charge increase of 4	.74	.39	.21	.016 (Λ_c --> p K π)
Efficiency for primary multiplicity cut of 9	.2	.2	.2	.2
Probability for both to decay in decay region	.26	.34	.45	.22
Trigger efficiency	.5	.5	.5	.5
Charm pairs on tape	61,000	43,000	7,500	1,640

	D^o, D^o	D^+, D^-	Λ_c --> p K π
Number on tape	166,000	58,000	1640
Acceptance	.88	.78	.97
Reconstruction efficiency x fraction analyzable	.25	.28	.60
Number reconstructed	36,000	13,000	950

Number of interactions	4.48×10^9
Number of triggers	4.48×10^7
Trigger rate	28 Hz

that a Λ_c-charged D pair get to the decay region is .27.

d. Λ_c's are produced about as frequently as charged D's. This result (from NA27[21]) also has large errors, and is based in part on the p K^- π^+ branching ratio. About 6/9's of all charm events should contain a Λ_c.

Based on this input, we expect about
$4.48 \times 10^9 \times .0016 \times 2/3 \times .86 \times .2 \times .5 \times .022 \times .20 \times 6/9 = 1210$
Λ_c's paired with neutral D's and another 430 paired with charged D's, all decaying to the p K^- π^+ mode. The final sample is 1640 Λ_c's.

7. Ξ_c **YIELD:** The Ξ_c has recently been observed in neutron-nucleus interactions[19]. The decay modes detected were Λ K π π and Σ^0 K π π and the x_F dependence reported was $(1-x_F)^6$. Net acceptance for this mode in the proposed experiment is .08, including a factor of .27 for the Λ (see Fig. 11). If the product of cross section times net branching ratio to these two modes is 1 microbarn (which seems to be consistent with the reported result), the yield would be 200 Ξ_c's. Yields to other decay modes, such as Σ^+ K^- π^+, may be even larger.

8. **RATES:** The trigger rate is 28 Hz and 44.8×10^6 events will be recorded on 4500 magnetic tapes.

5.2. YIELDS AND RATES FOR DIFFRACTIVE CHARM

We plan to run the part of the experiment to search for coherent diffractive production of charm for two weeks in a $.5 \times 10^6$ MHz 850 GeV proton beam. The yield calculation depends on many assumptions, and in particular on the estimate that the proton contains 0.3% intrinsic charm. Details are presented in Appendix II. If the estimates and assumptions prove correct, the yield would include about 800 Λ_c's to the p K^- π^+ mode alone and 4000 D's. The trigger rate is 25 Hz.

6. EVENT SELECTION AND RECONSTRUCTION

Initial event selection is implicit both in the operation of the trigger and in the charm sample used to calculate raw yields. Each of the charm particles in the pair must decay at least 0.6 mm. downstream of the target in the decay region, and into two or more stable charged particles. Offline analysis will be carried out in two passes, the first of which will use the Fermilab ACP. First pass cuts select events in which there are two or more tracks with impact parameters greater than 3 standard deviations away from the interaction vertex, and reject events in which there was a secondary interaction in one of the 'after'

multiplicity detectors. Monte Carlo studies show that these cuts retain more than 80% of the charm sample used to calculate raw yields; the cuts are estimated to retain 1% of the original sample, or 400,000 events. Second pass cuts will be based on vertex finding and fitting, and therefore include acceptance. We plan to analyze the charm decays which include 0 or 1 π^0 in addition to two or more stable charged particles. This selection criterion retains 40%[11] of the raw yield of D's. (Decays involving a Λ or K_s can also be analyzed, but are ignored in the following. Efficiency for these events is lower because the acceptance for the "V" , Fig. 11, is smaller than for other particles, because the "V" cannot be unambiguously assigned to a vertex, and because the 2 prong branching ratio is not unity.) Acceptance for the all charged modes varies from 97% for Λ_c --> p K^- π^+ to 78% for the D^+ --> K^- π^+ π^+. The probability that the decay will occur at least 4 standard deviations downstream from the rear of the target is used as a tentative cut, and it varies from 60% for the Λ_c decay to 84% for the D decay. Balance of P_T must be used in decays involving a π^0, and the additional factor required for reconstruction efficiency is estimated to be 0.6. Table I gives the estimated yield of fully reconstructed charm particles; entries include weighted averages of the quantities described above. Of the fully reconstructed charm 2/3 are to all charged modes and more than 90% of these are to a K and one or more π. Neutral D's account for 74% of the sample. It is important to emphasize that we plan to select charm events on the basis of topology alone; mass resolution and particle identification play no part in the procedure. If the cuts used for the entries in Table I prove inadequate, other topological handles will be used. A powerful cut is the requirement of another decay vertex; 85% of the charm candidates will have a second vertex formed by two or more accepted charged particles, and 75% of these vertices will be at least 4 standard deviations downstream of the target.

Particle identification is important for distinguishing among charm species. Unfortunately, the use of Cherenkov detectors would be impractical in this experiment because charm decay products generally have high momenta. For example, the average momentum of a proton from the accepted decays of Λ_c's produced with a $(1-x_F)^2$ distribution is 110 GeV/c. Similarly, our time-of-flight hodoscope will be useful for only a small subset of the data sample. In most cases, however, particle identification can be achieved with good efficiency by kinematic constraints alone. If the mass of a daughter particle is incorrectly chosen, the parent mass will be wrong. An example should suffice

to demonstrate the technique (which we also employ in E653). There exists a potential contamination of the decay Λ_c --> p K^- π^+ by the decay D+ --> K^- π^+ π^+. We are primarily interested in the Λ_c, so if all ambiguous cases are rejected, we lose those Λ_c's which are consistent with a D+ hypothesis when the proton is called a π^+. We have studied this case with a simple Monte Carlo simulation. Using the average mass resolution of 18 MeV for D's produced with a $(1-x_F)^2$ distribution, and eliminating D - Λ_c ambiguities between 1830 and 1930 MeV/c^2, the loss amounts to 21% of the Λ_c's with a 2.6% feedthrough of D's. (See Fig. 19) In fact such a simple procedure would not be used. The Λ_c and D samples would be simultaneously fit assigning probabilties and calculating mass resolution on an event-by-event basis. However, the example demonstrates that particle identifiers are not needed in all situations to identify charm particles.

Another source of contamination of Λ_c's is by D+'s and F's decaying to 3 charged prongs and 1 or more neutrals. The effect of this contamination can be reduced by requiring that the P_T of the parent equal the sum of the P_T's of the daughters. However, background will still be present and good mass resolution is important for extracting the signal.

It is important to bear in mind that the amount of feedthrough of other charm species into the Λ_c signal depends on ratio of the Λ_c inclusive cross section to the total inclusive charm cross section. According to the Lund model the x_F distribution for the Λ_c has a flat component which saturates the charm cross section at large x_F, where our trigger is most efficient. See Figs. 1, 2, and 8.

A final handle available to purify the Λ_c is the Σ_c --> Λ_c π cascade decays. As in the D* --> D π cascade decays, the π must be monoenergetic in the rest frame of the daughter charm particle. The doubly charged and neutral Σ_c decays have unique signatures that cannot be confused with a D* decay. How useful the handle actually is depends on the Σ_c/Λ_c cross section ratio. Summed over all charged states, the ratio for strange particles, Σ/Λ, is roughly .5 in 400 GeV/c proton copper interactions[4, 5]. If the ratio is the same for charm baryons, 1/3 of the Λ_c's originate from Σ_c decays.

7. COST ESTIMATES

7.1. COSTS TO FERMILAB

1. PREP electronics: $150K
2. Surveying: $10K
3. Analysis time on 100 node ACP system: (1000 hours)
4. Technician: (6 months)
5. Liquid argon and nitrogen for calorimeter: $35K

7.2. COSTS TO EXPERIMENTERS

1. Multiplicity jump trigger: $100K
2. Drift chamber rate upgrade: $10K
3. Vertex detector upgrade: $120K
4. Beam detector upgrade: $40K
5. Detector gasses: $50K
6. Magnetic tapes: $80K
7. Computing hardware: $30K
8. Apparatus repairs: $40K
9. Operating costs for 6 months: $140K
10. TOTAL: $610K

8. SCHEDULE

1/1/87--5/10/87

Purchase detectors and front end electronics for trigger. Design of level 2 electronics for multiplicity jump trigger. Prepare for second emulsion run of E653

5/11/87--10/11/87

Second emulsion run of E653. Test parasitically the multiplicity jump triggers. Test rate capability of drift chambers.

10/12/87--3/31/88

Complete trigger electronics. Upgrade drift chambers for high rate.

4/1/88--7/31/88

Third emulsion run for E653.

8/1/88--8/31/88

First run of proposed experiment

9/1/88--1/31/88

Upgrade vertex detector.

2/1/89--6/30/89

Second run of proposed experiment.

9. APPENDIX I. PREDICTED PERFORMANCE OF THE MULTIPLICITY JUMP TRIGGER

9.1. SILICON WAFER TESTS

In August, 1985 during the first run of E653 we evaluated a prototype multiplicity jump trigger. Beam was obtained parasitically from the experiment (E711) upstream of ours by channeling in a bent silicon crystal. Fig. 20 shows the prototype device. It consisted of an upstream interaction veto detector, a 3/16" long graphite target, a pair of 'before' multiplicity detectors, a 1" decay region, and finally 6 'after' multiplicity detectors. All detectors were 300 micron thick silicon wafers with a 14 mm. square active area. Data from tests carried out on the prototype can be used to predict the performance of the multiplicity jump detector to be used in this experiment.

Two remarks should be made about the pulse height distributions obtained in the silicon detectors. The first is that the most probable energy loss per minimum ionizing particle rises logarithmically as the number of particles simultaneously passing through the detectors increases[30]. For a single particle it is 86 KeV; for 10 particles it is 100 KeV. The energy loss spectrum for a single particle is accurately described by an empirical model[30, 31] which takes into account atomic effects by convoluting a Gaussian with the Landau distribution. All pulse height distributions discussed in the following are normalized to the most probable pulse height (not the average) for a single minimum ionizing particle; the resulting normalized unit pulse height is called a 'mip'.

The second remark is that predicted energy loss is not the same thing as energy deposition. This fact gives rise two experimentally significant effects. One is that the Landau 'tail', for which single delta ray production is the main contribution, disappears when the number of particles passing through a detector is large. The delta rays are sufficiently energetic to escape from the detector. The other is that in a stack of dectectors the width of the pulse height distribution is larger than predicted by the model. Delta rays produced by one detector can enter another, so that the stack is in a sea of delta rays. We observed both effects in our tests.

The tests of the prototype showed that use of wafers rather than SSD's in a multiplicity jump trigger would be feasible. (However, it is less efficient because of the larger effects due to spallation protons, and provides a poorer handle for background

suppression.) To minimize fluctuations we used as the estimators of multiplicity the wafer with the minimum pulse height in the 'before' group (wafers 2 and 3) and that with the minimum pulse height of the first 4 in the 'after' group (wafers 4, 5, 6, and 7). Fig. 21 is a plot of 'after' – 'before' obtained in this way. The long tail on the left of the distribution is due to spallation protons entering the 'before' wafers. If a cut is placed at 3, the efficiency for charm would be 22% and the background trigger rate would be 1.2%.

9.2. ESTIMATES FOR MULTIPLICITY JUMP TRIGGER PERFORMANCE

To estimate how well the multiplicity jump trigger described in the proposal would work for charm only the wafers at the downstream end of the decay region were used (see Fig. 20). In these wafers the effects of spallation protons can be ignored. Cuts on pulse heights in wafer 1 (< 1.4) and 2 and 3 (both > 2.5) assured no interaction upstream of the target and an interaction in the target.

The operation of the proposed multiplicity jump trigger was 'simulated' by calling wafer 7 the detector upstream of the decay region and wafers 8 and 9 the detectors downstream of the decay region. Fig. 22 shows the pulse height in wafer 7 (it looks peculiar at the low end because of the interaction requirement and some non-interacting beam). The pulse height in wafer 7 was required to be greater than 2.5 to further suppress non-interacting beam. The pulse height was also required to be less than 13, approximately the median of the distribution. The proposal discusses a cut of 9 particles entering the decay region, where 9 is about the median of the multiplicity distribution. Due to Landau fluctuations and the logarithmic rise mentioned above, the normalized pulse height cut in wafer 7 must be greater than 9 mips to have efficiency for 9 particles. In order to understand in more detail what this cut does, it is necessary to look at wafers 8 and 9. To get the best estimator of the most probable pulse height (i.e., suppress Landau fluctuations) the wafer with the minimum pulse height (min(8,9)) is used. Fig. 23 is the ratio of the pulse height distribution of min(8,9) after the cut on wafer 7 to that before; it shows the probability that an event survive the upper limit cut as a function of the number of particles entering the decay region. Here, the logarithmic rise is again important; the most probable pulse height for 9 particles is 10.5, where the efficiency is 72%. Since there is some efficiency above 9 particles, the approximation that the upper level cut is 100% efficient for 9 or fewer particles and 0% above is used in the proposal.

Fig. 24 is a histogram of min(8,9) - wafer 7 pulse heights. In this case the logarithmic rise is not particularly important. If a cut is put at 3 particles, about 2% of the events in the histogram would pass the cut. A multiplicity jump of 4 in the decay region (between wafers 7 and 8) would be equivalent to shifting the whole distribution to the right by 4 units and 61% would pass the cut.

The proposed multiplicity jump trigger will use an SSD in place of wafer 7. Although in one dimension the trigger will select strips to subtend the same angle at the target as the wafers (+/- 300 mr), in the other dimension the angle will be pi radians. In about 20% of the events a spallation proton will still enter the device[23]. It is assumed that these events will be lost. Thus the estimate of 50% efficiency for a multiplicity jump of 4. Note also that in the proposed device the initial and final multiplicity detectors will not subtend the same angle parallel to the strips. This is not particularly important in so far as both have sufficient acceptance to detect essentially all high energy particles.

10. APPENDIX II. ESTIMATES FOR COHERENT DIFFRACTIVE PRODUCTION OF CHARM

1. BEAM: We plan to use a 500 kHz 850 GeV proton beam and run for two weeks, or 2 x 10^5 seconds of beam.

2. TARGET: The target will be a 1% absorption length stack of silicon wafers. The interaction rate is 5 kHz, and the total number of interactions is 10^9.

3. CROSS SECTION: In order to estimate the cross section, we need to know the total coherent diffraction dissociation cross section for protons off silicon. This can be obtained from proton-proton data using factorization[16]. Final state interactions and energy dependence of the diffractive cross section are ignored. With these simplifications, the fraction of the total cross section which is diffractive dissociation equals that in proton-proton collisions (in which only the beam proton is dissociated) times the following cross section ratio:
(total elastic/total for silicon)/(total elastic/total for protons).
The result is that the total coherent diffractive dissociation cross section is 15% of the total cross section for silicon. Next, the cross section must be integrated over the mass of the diffractive state from charm threshold to the coherence limit for silicon. The upper limit, 13 GeV, corresponds to a t_{min} which equals the slope parameter, 0.012, for coherent single scattering.
$d\sigma/dM^2 = const/M^2$,
for diffraction between M^2 of 1.5 and the coherence limit[16]. Integration between these limits gives the total diffractive cross section. The integrated cross section for which charm pairs can be produced is about half of the total diffractive dissociation cross section. We assume that in this mass region charm will be produced 0.1% of the time. Brodsky et al.[9] estimate that the proton contains 0.3% charm. Our assumption is more conservative to take into account threshold and end effects. Thus, the probability of producing coherent diffractive charm is estimated to be 7.5 x 10^{-5}/interaction (about 5% of the total charm production cross section), and we would produce 75000 pairs of charmed particles.

4. TRIGGER ACCEPTANCE: We choose a benchmark pair consisting of a Λ_c and a neutral D, and assume that all charm produced consists of this pair. Only the p K π mode (branching ratio 2.2%) of the Λ_c is used in the estimates. The D is required to decay to two or more charged prongs, which occurs 86% of the time[27]. If, on the average, each charm particle carries half the beam momentum, the probability that the pair reach the decay region is 69%. The average number of charged particles accompanying the charm pair is 2.5[16]. Of the charm pairs that enter the decay region 80% survive the cuts that the multiplicity jump be 3 or greater and that the number of charged particles entering the decay region be less than 6.

5. NET YIELD: The net yield of Λ_c's to the p K π mode alone is estimated to be:
   75,000 x .022 x .86 x .69 x .8 = 783
   If the branching ratio of the Λ_c into three prongs is 25%, the charm yield would also include 4000 D's to modes consisting of two or more stable charged particles and not more than one π^0. The trigger rate is 25 Hz.

References

1. M. Aguilar-Benitez et. al.,. CERN/EP 85-118
2. M. Aguilar-Benitez et. al.,. Phys. Lett. 123B, (1983), 103
3. T. Sjorstand,. Phys. Lett., 142B, (1984), 420
4. L. G. Pondrom. Phys. Rep., 122, (1985), 57
5. T. R. Cardello, et al.. Phys. Rev., 32D, (1985), 1
6. S. F. Biagi, et al.. Phys. Lett 122B, (1983), 455
7. S. Reucroft. Hadroproduction Characteristics of Charm and Beauty, to appear in Proceedings of Sixth International Conference on Physics in Collision
8. R. Ammar, et al.,. CERN/EP 86-122
9. S. Brodsky, et al.,. Phys. Lett. 93B, (1980), 451
10. S. Brodsky,. SLAC-PUB-3770
11. Particle Data Group,. Review of Particle Properties in Phys. Lett., 170B, (1986), 1
12. E. Berger, et al.,. ANL-HEP-PR-86-14
13. G. Ingelman and P. Schlein,. Phys. Lett., 152B, (1985), 256
14. H. Fritzsch and K. Streng,. MPI-PAE/PTh 53-85
15. S. J. Brodsky. SLAC-PUB-4018
16. K. Goulianios,. Phys. Rep., 101, (1983), 169
17. J. C. Anjos, et al.. FERMILAB-Pub-86/155/E
18. R. Padley. Talk given at the 1987 Meeting of the Division of Particles and Fields of the American Physical Society, Salt Lake City, Utah
19. P. Coteus, et al.. COLO-HEP-140
20. R. Bailly, et al.. Zeit. Phys., 30C, (1986), 51
21. S. Reucroft,. private communication
22. P. Weilhammer,. Talk given at the 6/25/85 meeting of the Fermilab Heavy Quark Working Group
23. K. Braune, et al.,. Z. Phys., 13C, (1982), 191
24. G. Bellini, et al.,. Nucl. Inst. and Meth., 107, (1973), 85
25. R. Ammar, et al.. CERN/EP 86-122
26. S. Reucroft,. private communication
27. M. Aguilar-Benitez, et al.,. Phys. Lett., 135B, (1984), 237
28. G. Abrams, et al.,. Phys. Rev. Lett., 44, (1980), 10
29. J. Bjorken. private communication
30. S. Hancock, et al.,. Phys. Rev., 28A, (1983), 615
31. S. Hancock, et al.,. CERN EP/83-138

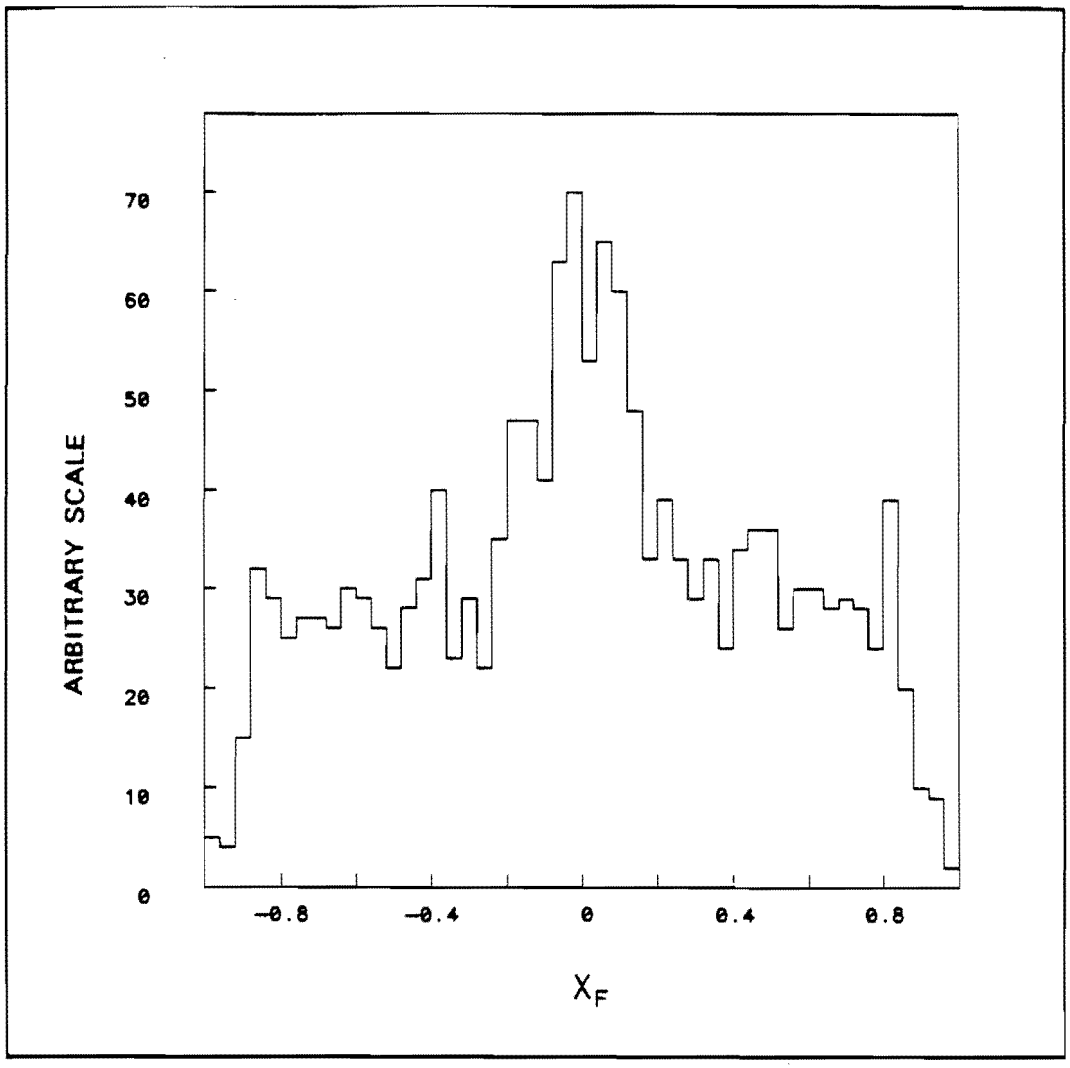

FIGURE 1. The x_F distribution for Λ_c's predicted by the Lund model. Results are from the Lund Monte Carlo.

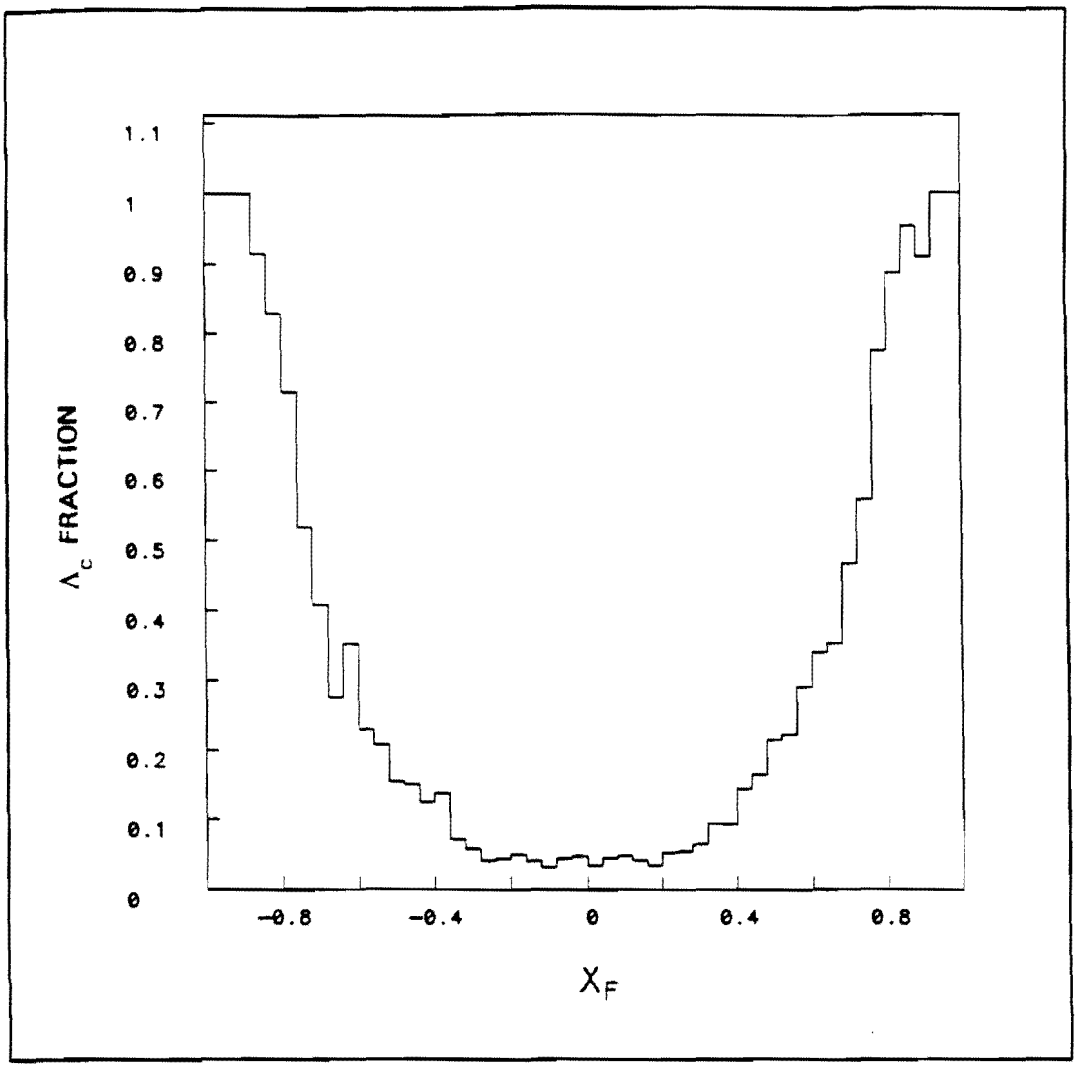

FIGURE 2. The fraction of the total inclusive charm cross section which is Λ_c's. The results are predicted by the Lund model and obtained with the Lund Monte Carlo.

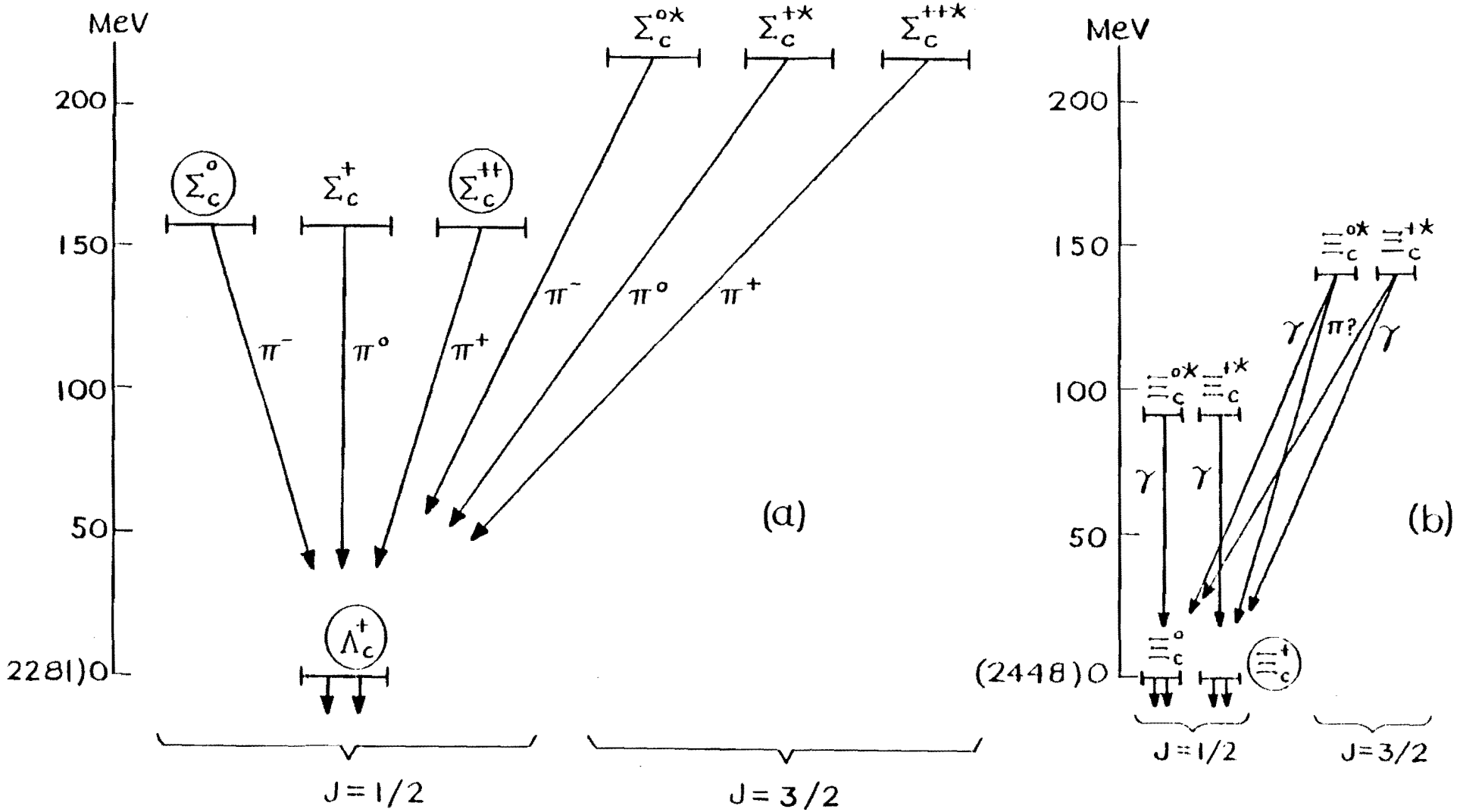

FIGURE 3. Low lying charm baryon levels (adapted from A. De Rujula, et al., Phys. Rev. 12D, 147, (1975)). (a) Charm baryons. (b) Charm-strange baryons. Only the encircled states have been observed. Note that good π^0 and photon detection are required to observe many of the states, particularly those which have not yet been found.

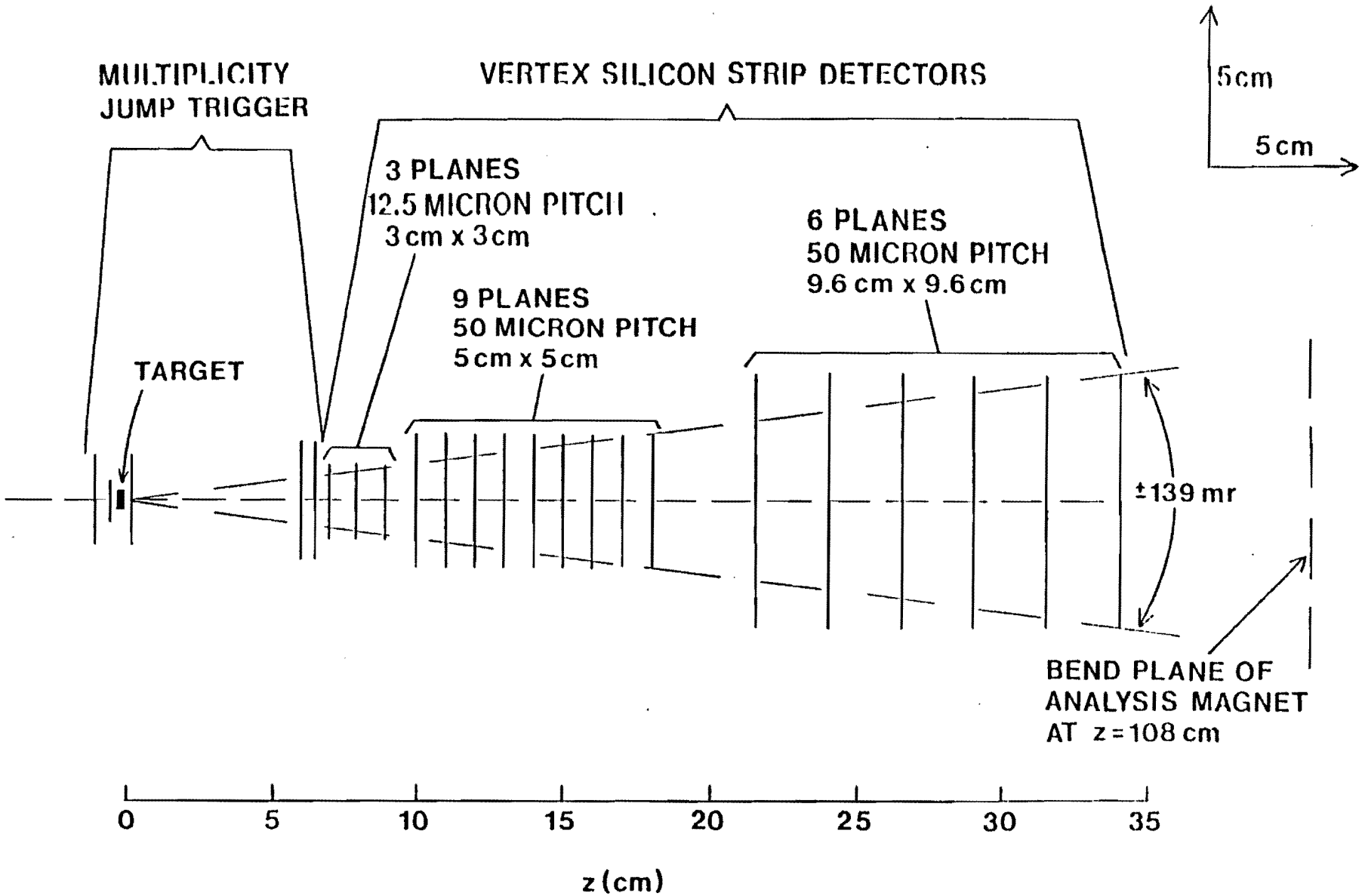

FIGURE 4. Target region and vertex detector of proposed experiment

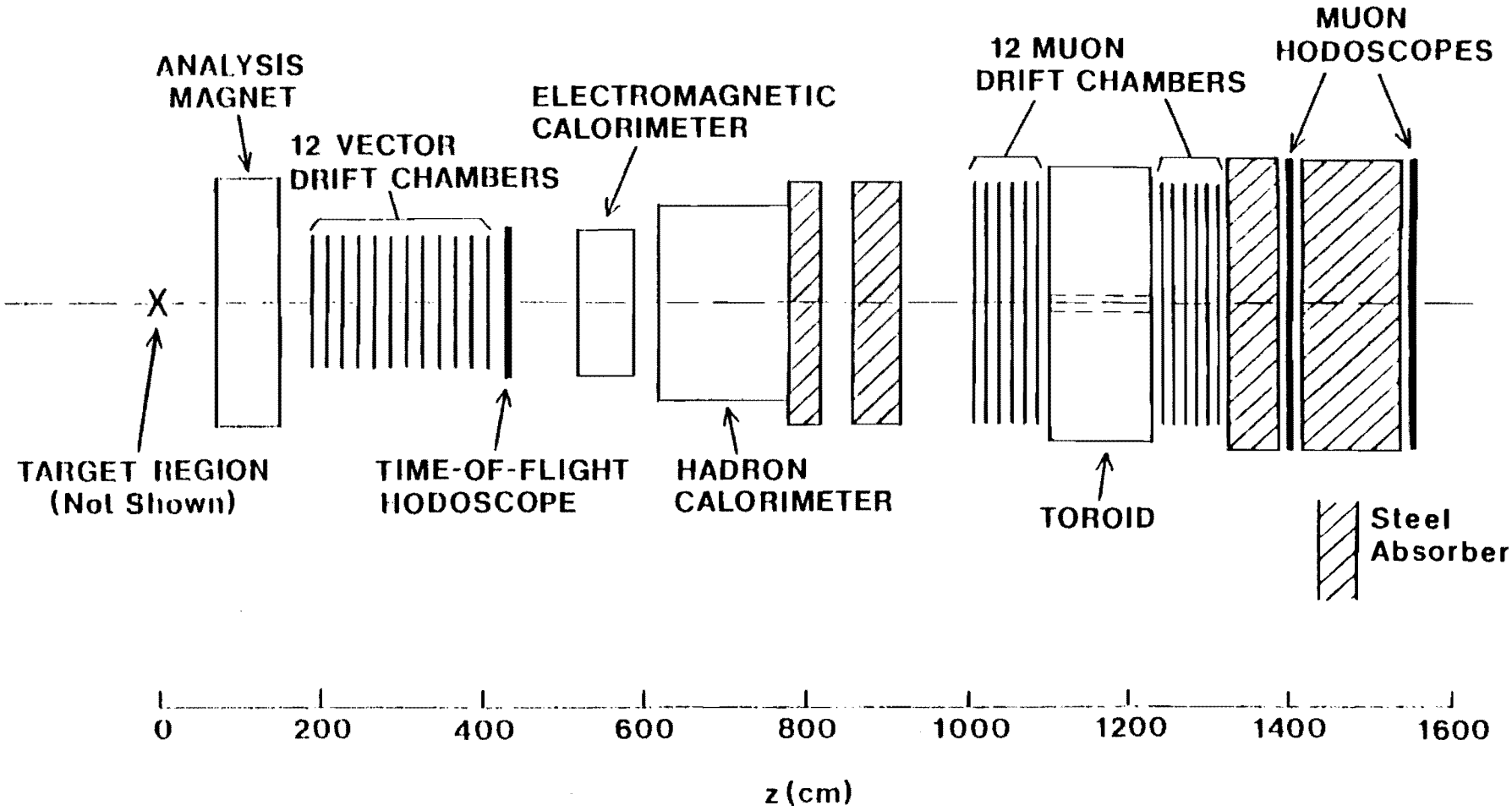

FIGURE 5. Plan view of the apparatus to be used in proposed experiment.

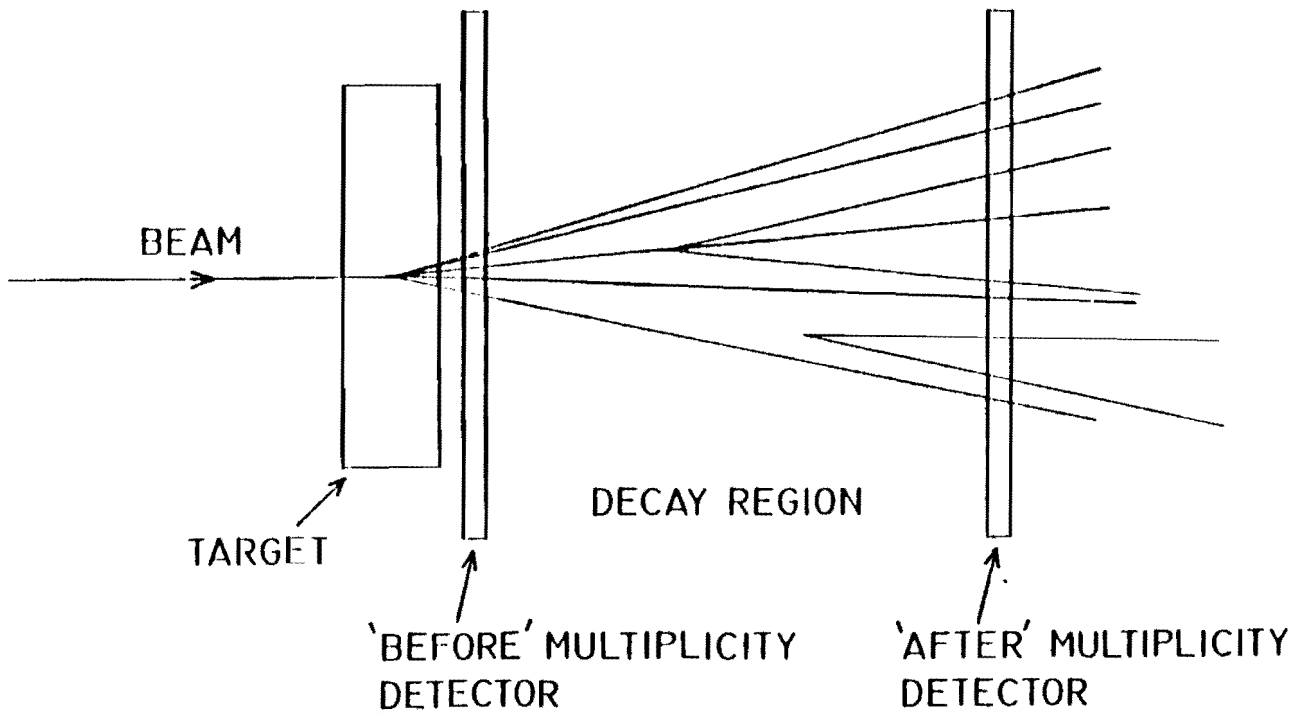

FIGURE 6. Schematic illustrating the basic principle of the multiplicity jump technique. A pair of charm particles is shown decaying in the decay region. Multiplicity at the 'before' detector is 5; at the 'after' detector it is 9.

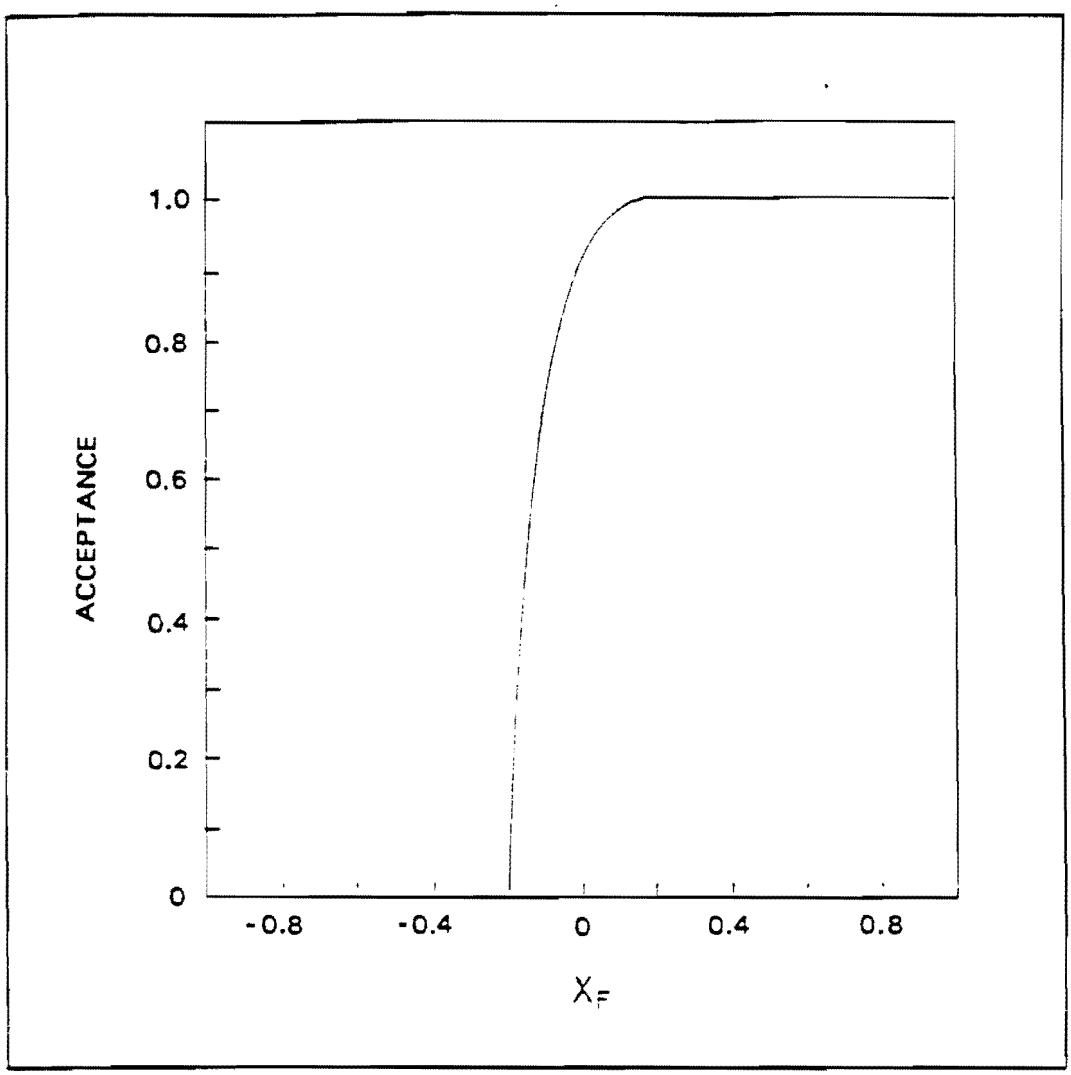

FIGURE 7. Spectrometer acceptance for the decay Λ_c --> p K π. The curve is the result of a Monte Carlo simulation.

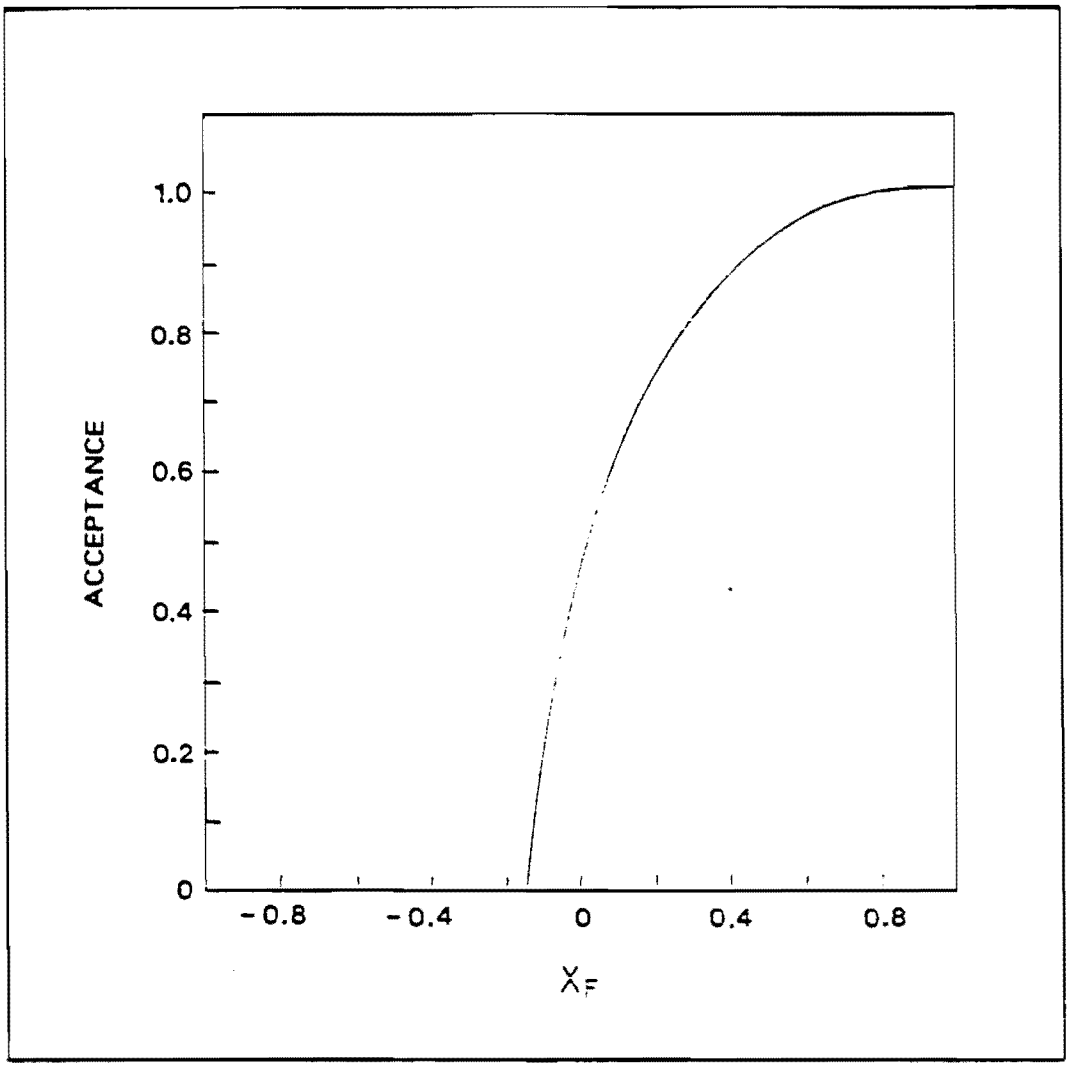

FIGURE 8. Net acceptance for Λ_c --> p K π. The acceptance is the joint probability that the Λ_c reach the decay region of the multiplicity jump trigger and that all three decay products be accepted by the spectrometer. The curve is the result of a Monte Carlo simulation.

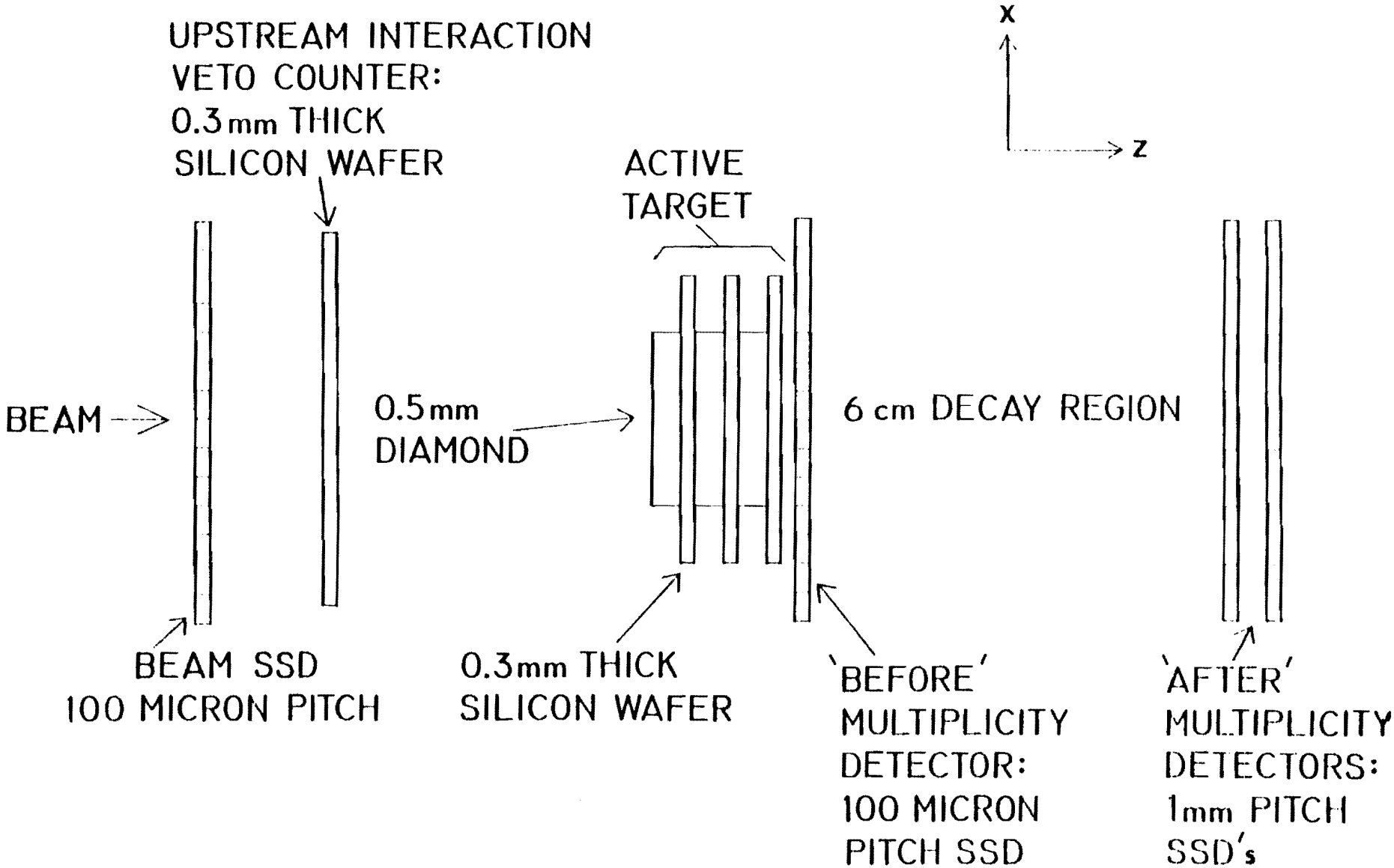

FIGURE 9. Schematic of proposed multiplicity jump trigger. The drawing is not to scale.

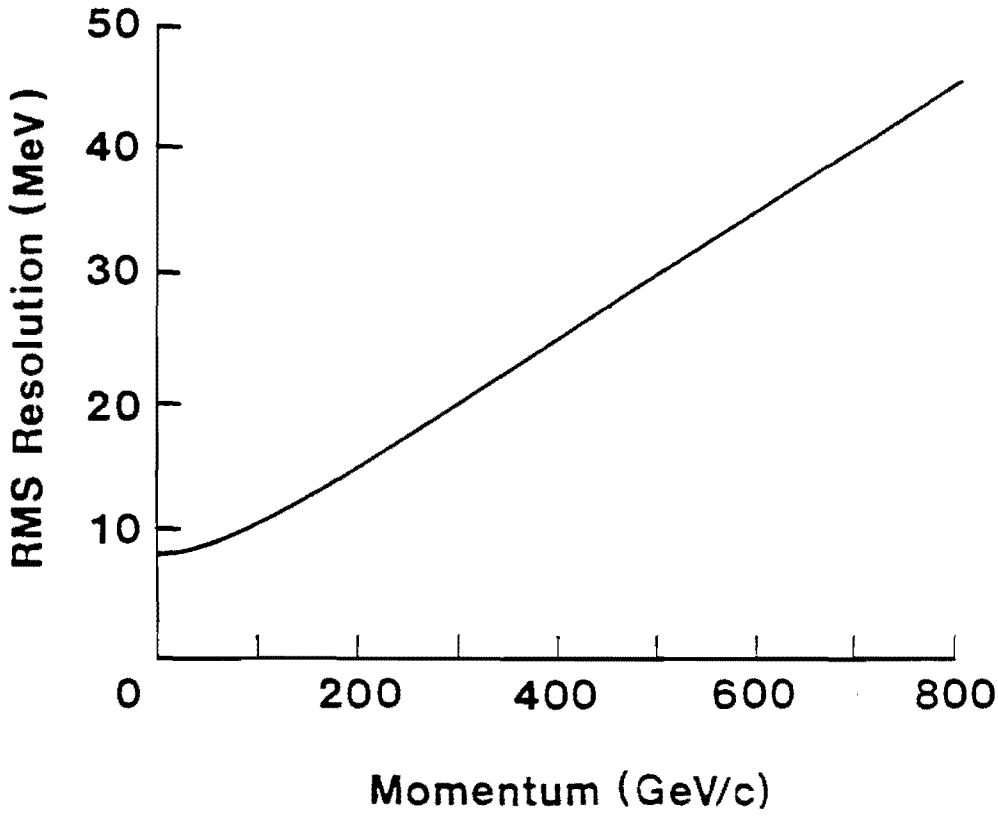

FIGURE 10. RMS mass resolution for the decay $\Lambda_c \longrightarrow p\ K\ \pi$. The curve is a smoothed Monte Carlo result.

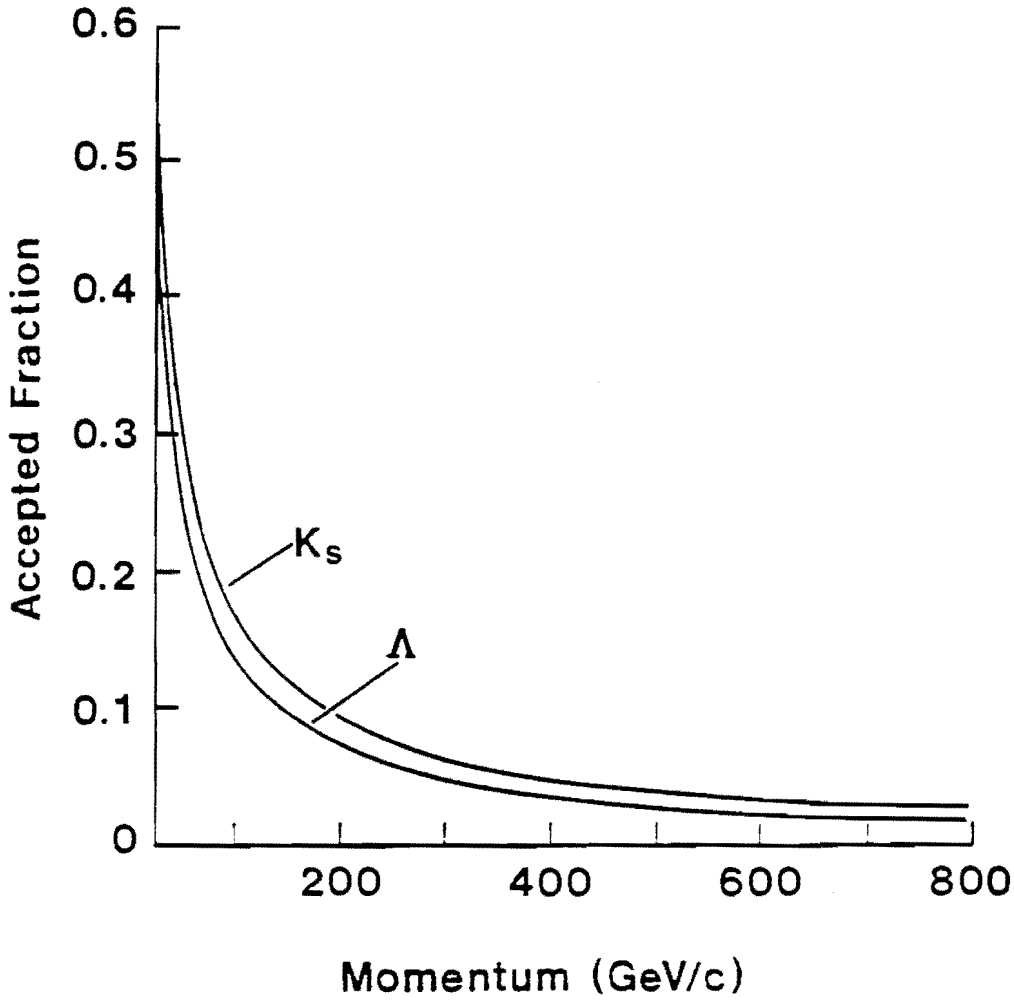

FIGURE 11. Neutral "V" acceptance for the proposed apparatus.

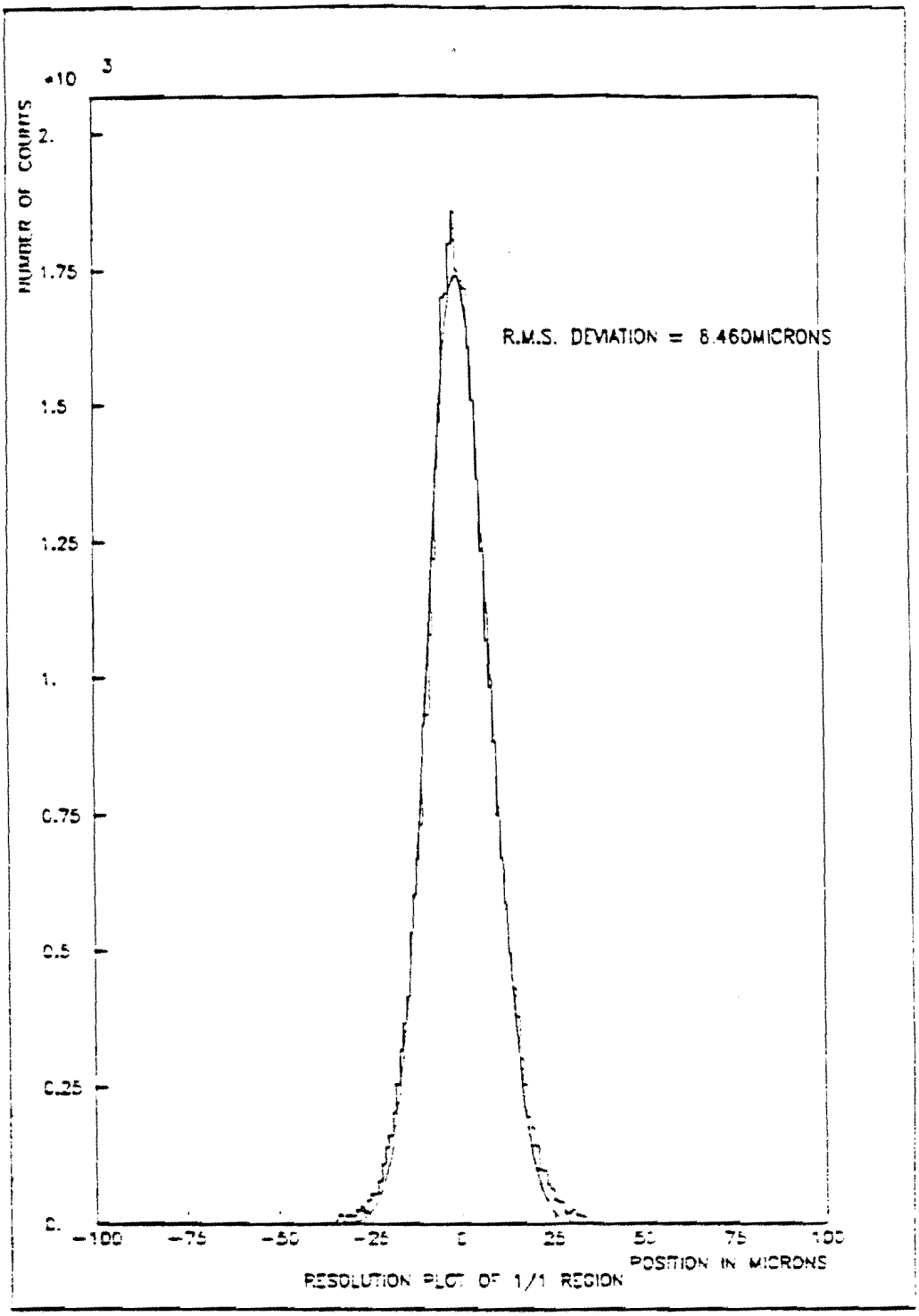

FIGURE 12. Resolution of the central region of one silicon strip detector. Data are from non-interacting beam tracks obtained in the 1985 run of E653.

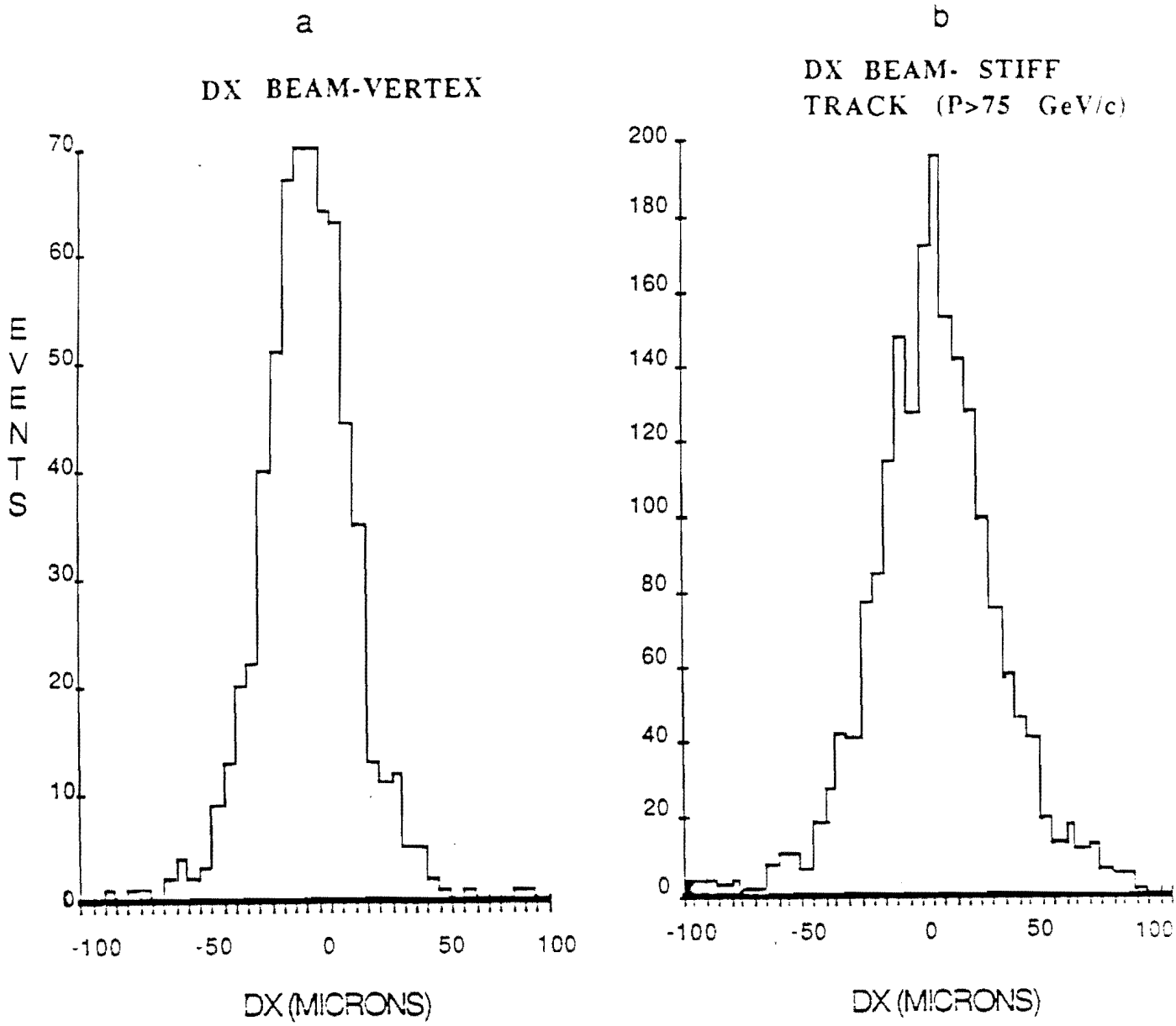

FIGURE 13. (a) Separation in x at the front of the target between beam trajectory measured by beam system and by vertex detector. Data are from non-interacting beam tracks. (b) Impact parameter distribution in the x - z plane for tracks with momentum greater than 75 GeV/c. These tracks are in region of the vertex detector with the highest track density. The similar resolutions of (a) and (b) show that the vertex detector can reconstruct tracks correctly even in a very busy environment.

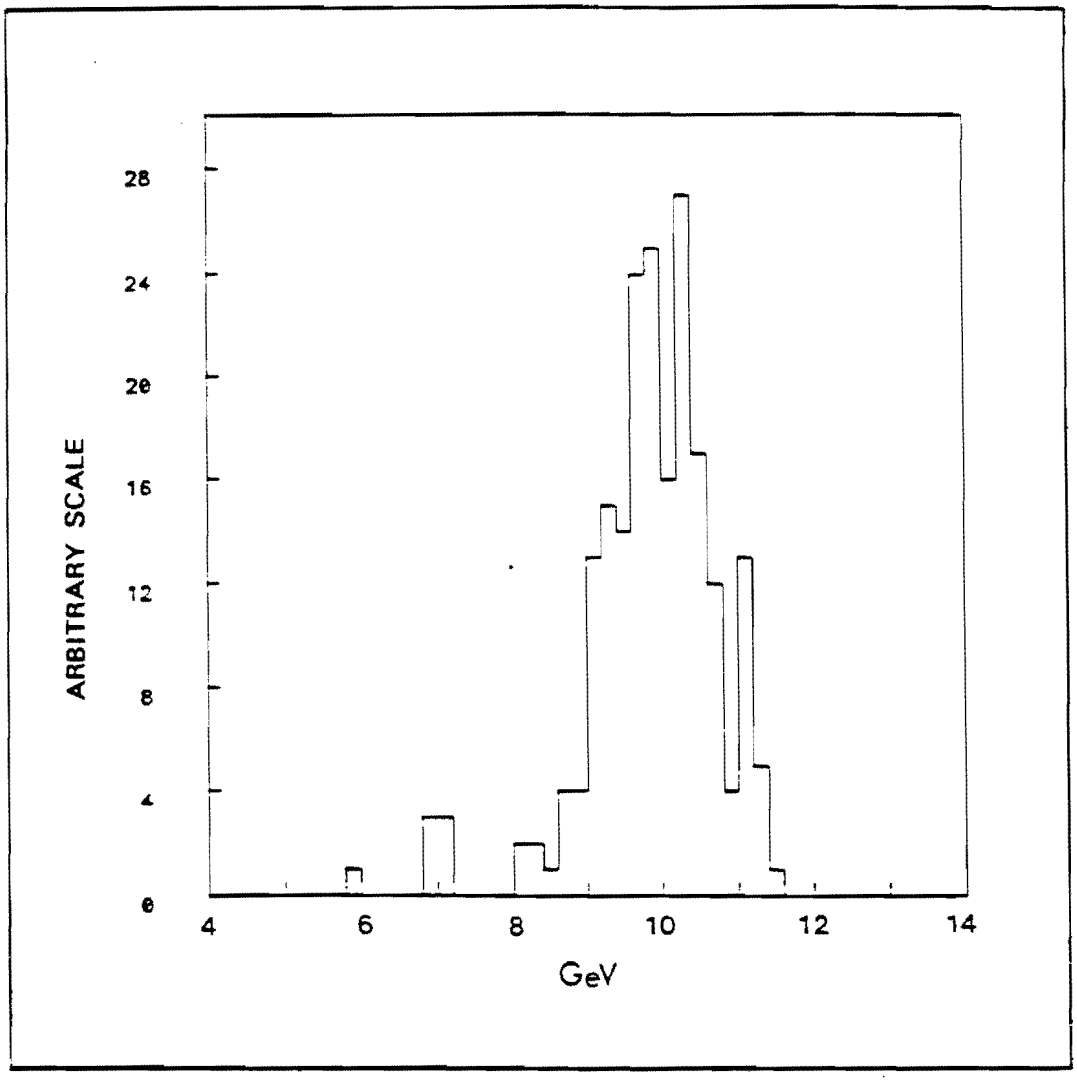

FIGURE 14. Energy resolution of liquid argon calorimeter for 10 GeV electrons. Data are from calibration beam and were collected during the 1985 run of E653.

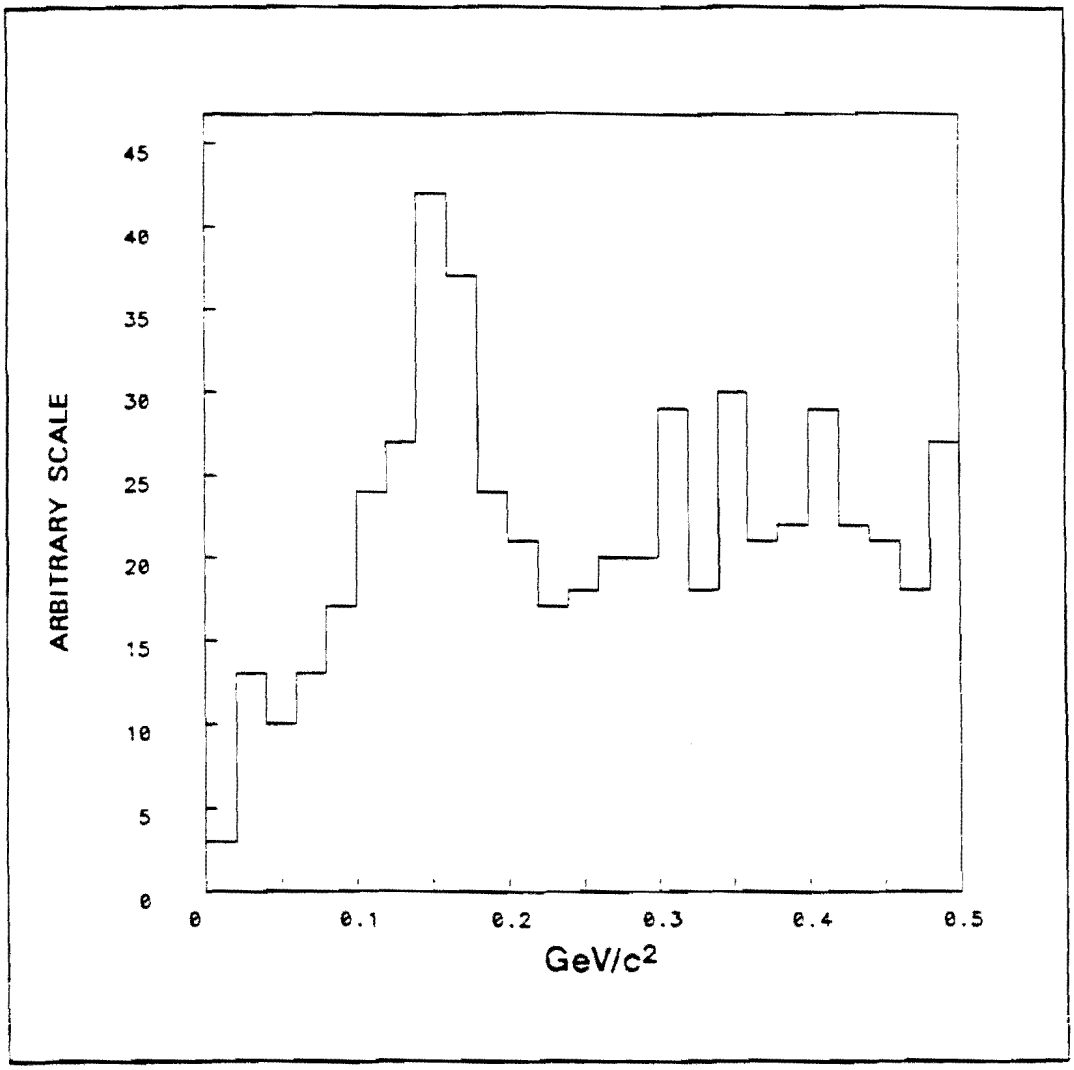

FIGURE 15. Di-photon mass resolution of liquid argon calorimeter in the mass region of the π^0. Data are from 1985 run of E653.

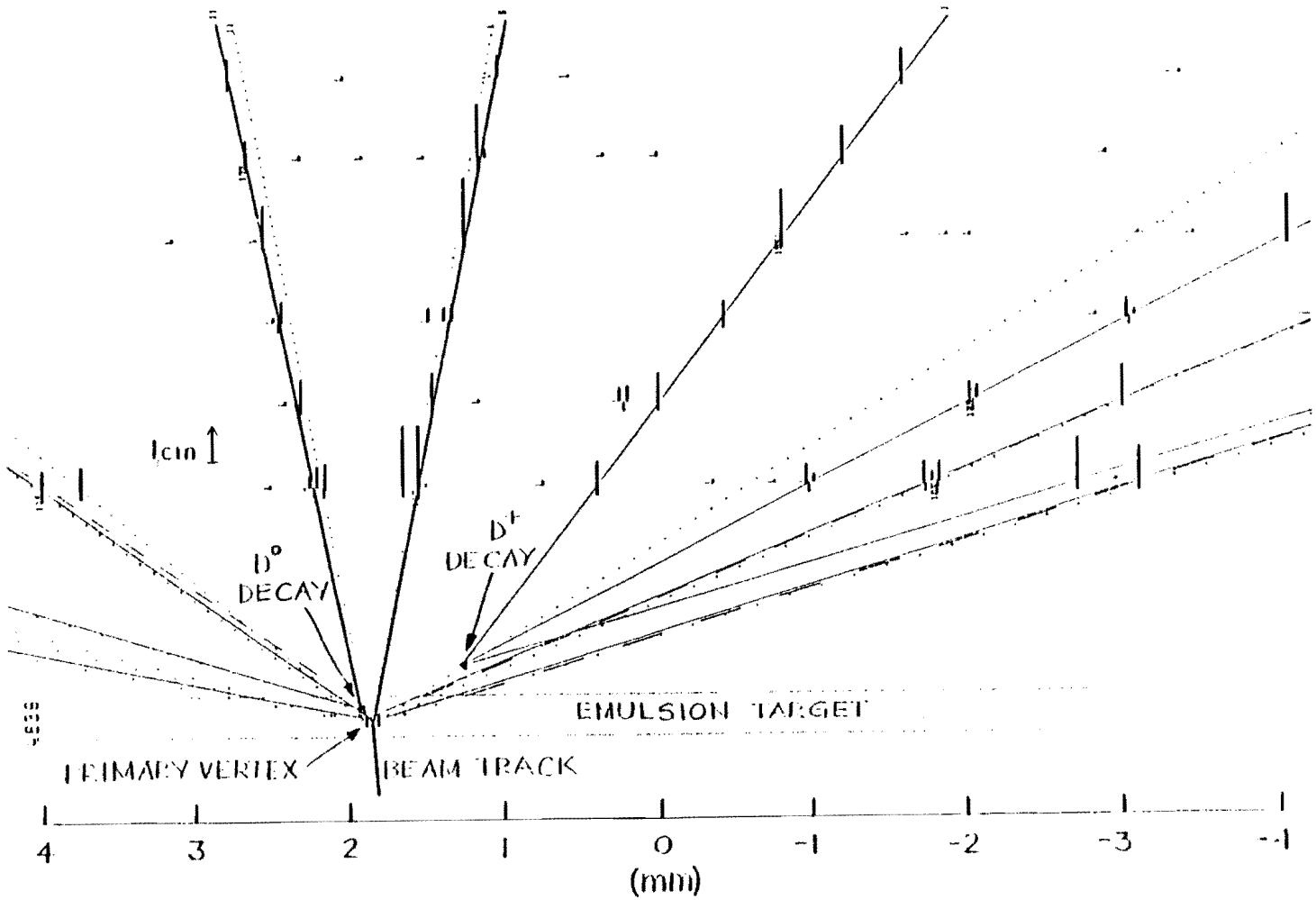

FIGURE 16. An event display for the 'v' view of the vertex detector SSD's. The event is from the 1985 run of E653, and has two reconstructed charm decay vertices. Heavy lines on the downstream side of the detector planes are pulse heights. Light lines on the upstream side are hit positions calculated from the pulse heights. Tracks drawn with solid lines are those which have three dimensional fits in both the vertex detector and the spectrometer drift chamber system and have matched at the midplane of the analysis magnet. Tracks drawn with dashed lines have fits in the vertex detector, but no matching tracks in the drift chambers. Tracks drawn with dotted lines are projected from the nuclear emulsion target. The scale is in mm.

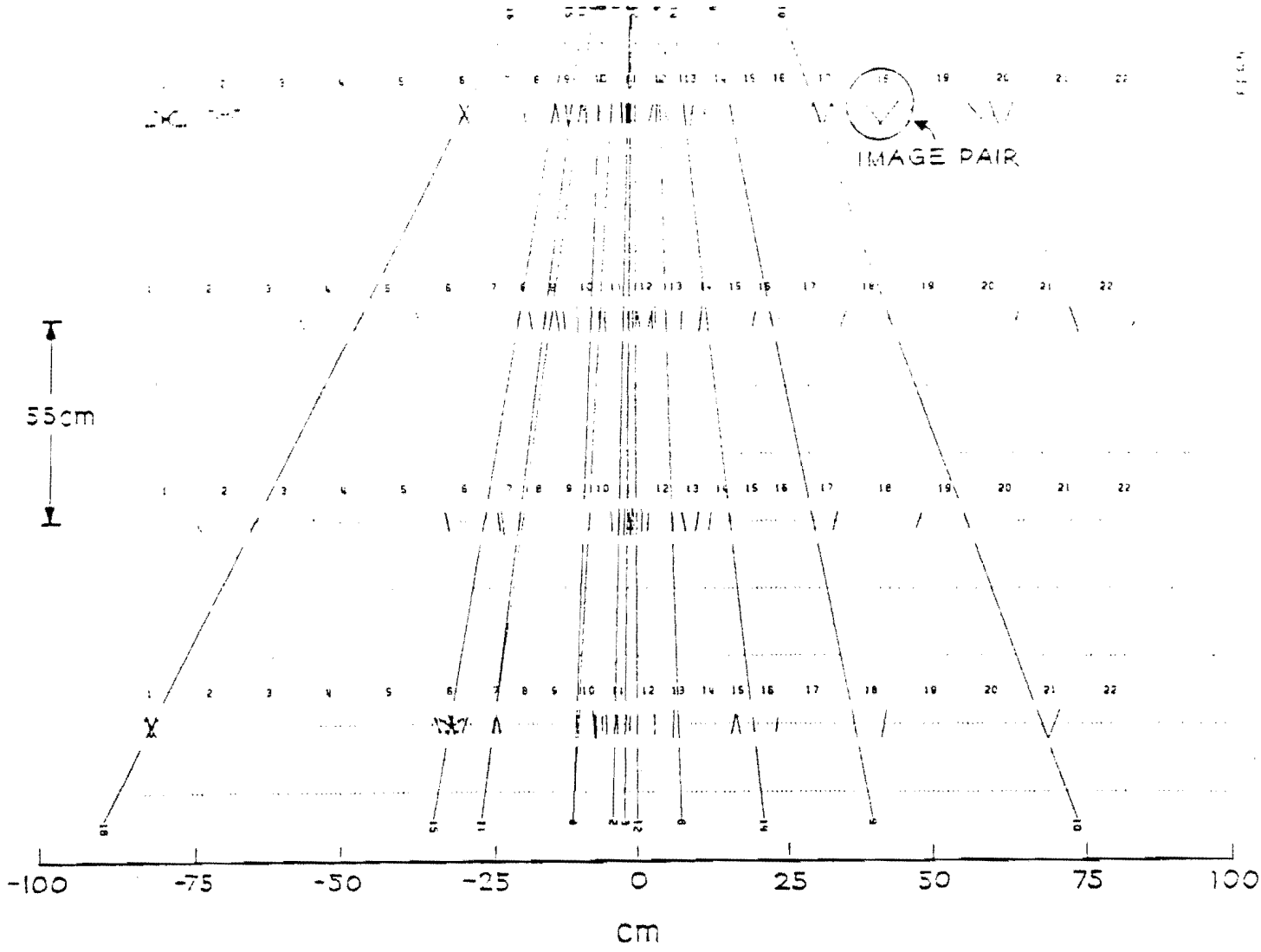

FIGURE 17. An event display for the 'u' view of the spectrometer drift chambers. The event is from the 1985 run of E653 and shows the same charm event as in Fig. 16. The small dark lines centered on the detector planes are the 'mini-vectors' and their mirror images. The numbers along the planes are drift cell indices. All tracks shown are the result of three dimensional fits. The event display shows clearly that several hits per drift cell can be accomodated and that crossing tracks are correctly handled. The important role of the 'mini-vectors' in pattern recognition is obvious from the display.

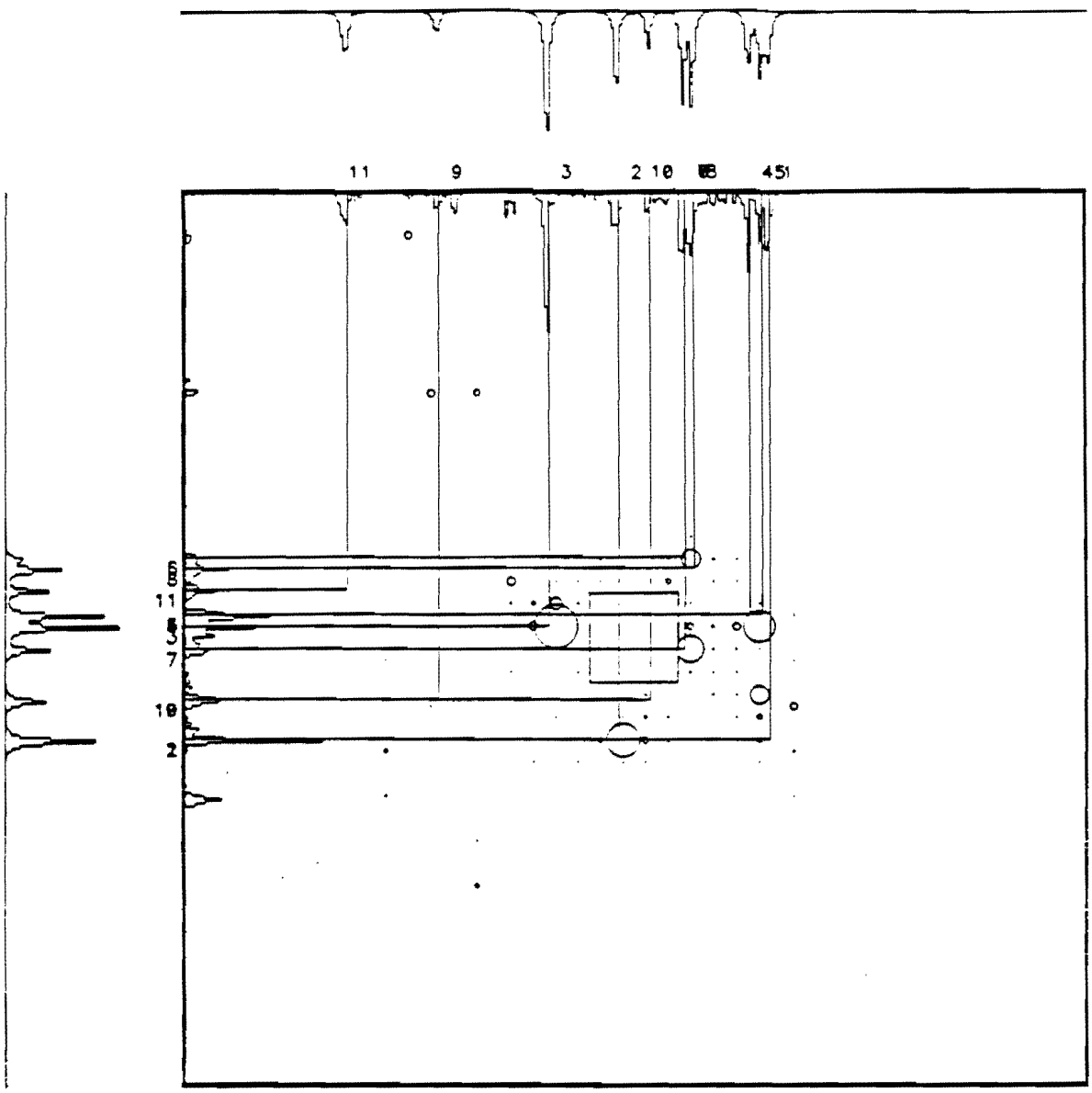

FIGURE 18. An event display for the front section of the liquid argon calorimeter. Measured pulse heights for the x and y views are displayed on the inside edges of the large box. Pulse heights of the pads are represented as circles centered on the pads. The diameter of a circle is proportional to the pulse height. The central small box is the region of the detector which is segmented entirely into small pads; information from it is not displayed. Results of pattern recognition are shown as intersecting lines inside the box and predicted shower shapes outside the box. The display shows that showers overlapping in one view can be resolved in software by using pulse height information in the pads.

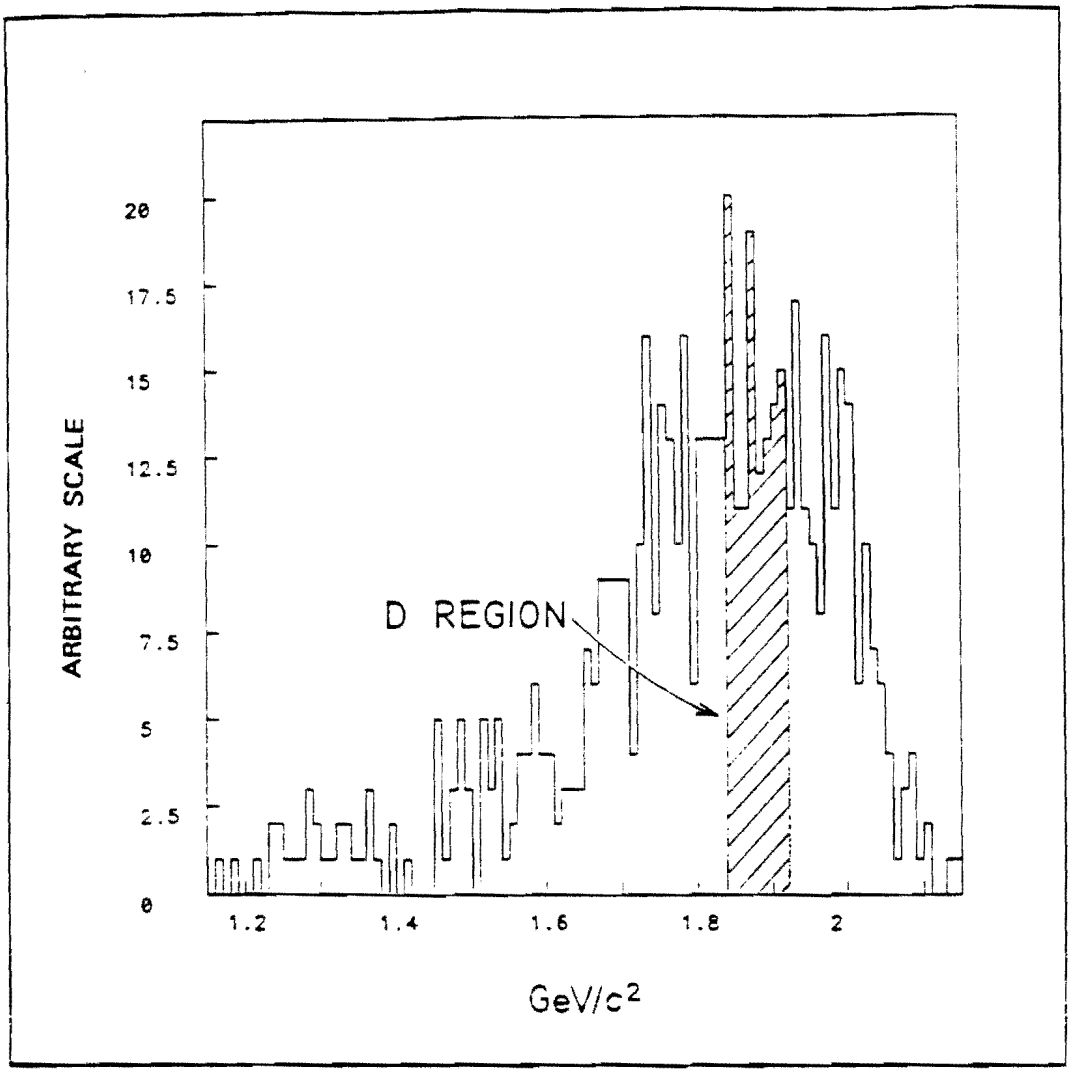

FIGURE 19. Mass distribution for the Λ_c --> p K^- π^+ decay when the proton is misidentified as a pion. The region where the decay can be ambiguous with a D --> K^- π^+ π^+ decay is cross hatched. The curve is from a Monte Carlo simulation.

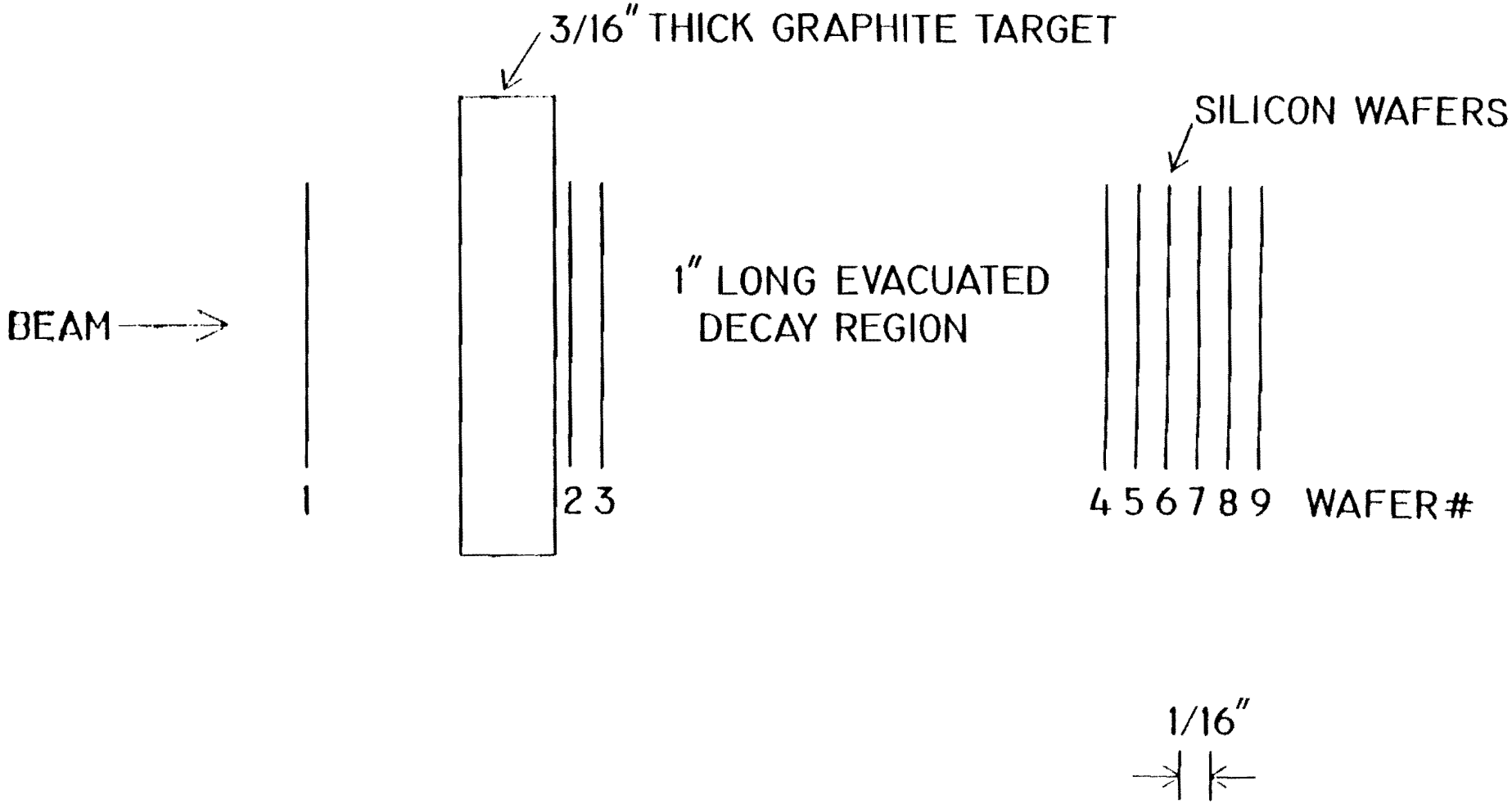

FIGURE 20. The prototype multiplicity jump trigger evaluated parasitically during the 1985 run of E653.

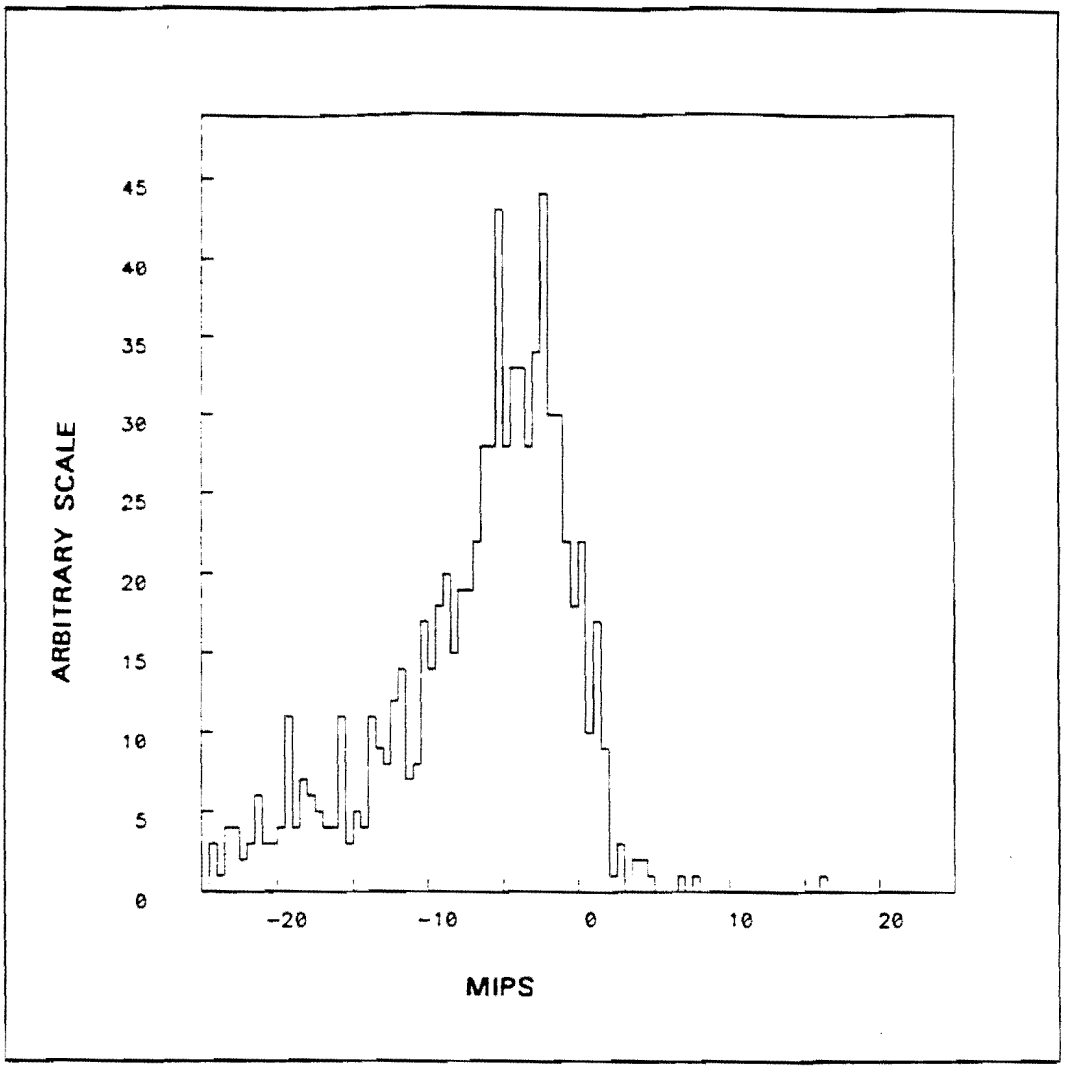

FIGURE 21. Performance of the prototype multiplicity jump trigger. The histogram shows the 'after' - 'before' pulse height difference distribution in the two groups of silicon detectors bracketing the decay region. See text for details. Data were obtained during the 1985 run of E653.

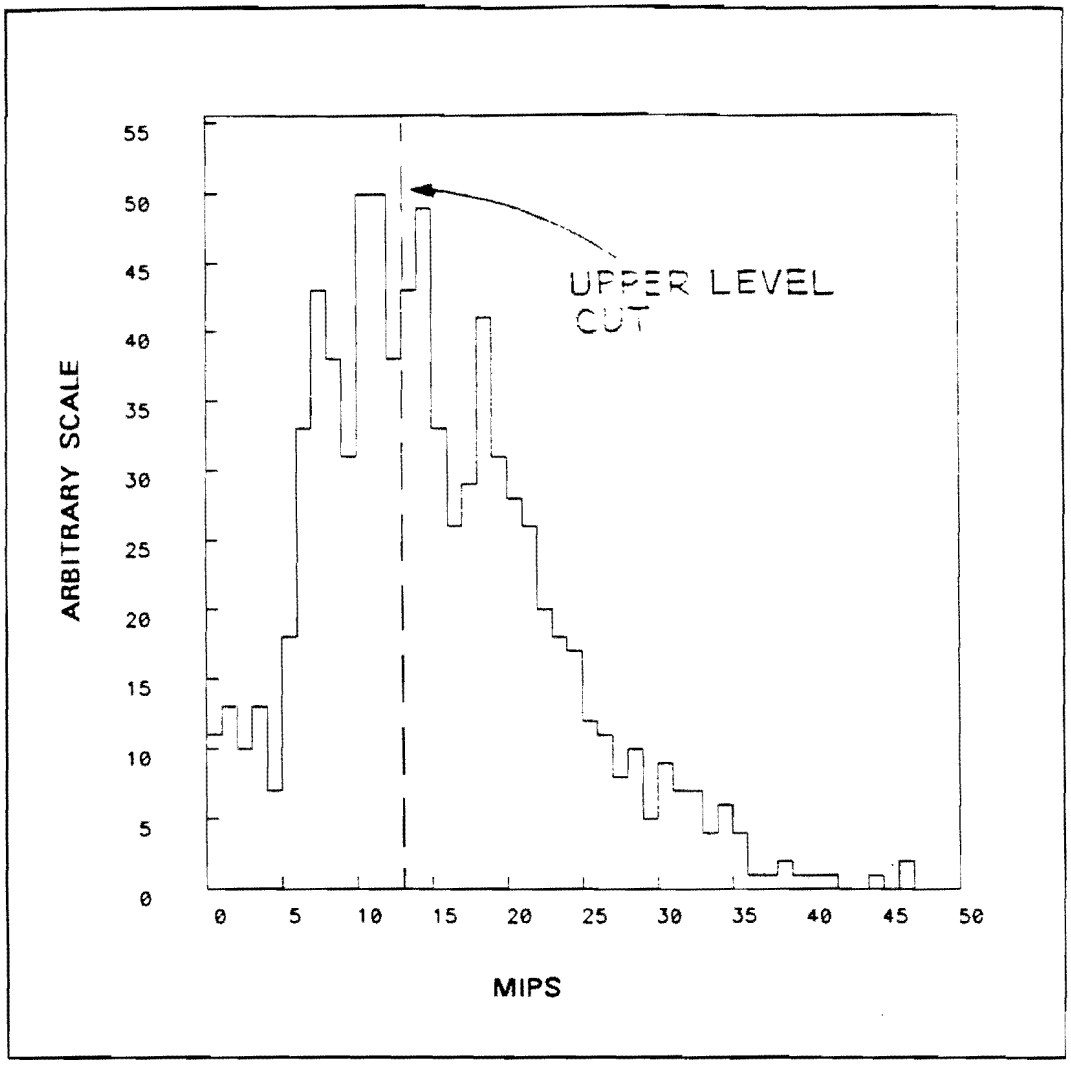

FIGURE 22. The pulse height spectrum of wafer 7 of the prototype for interactions in the target. Wafer 7 is used to simulate the performance of the 'before' detector in the proposed multiplicity jump detector. Non-interacting beam distorts the spectrum for small pulse heights. Only events below the upper level cut at 13 mips are accepted. Data were obtained during 1985 run of E653.

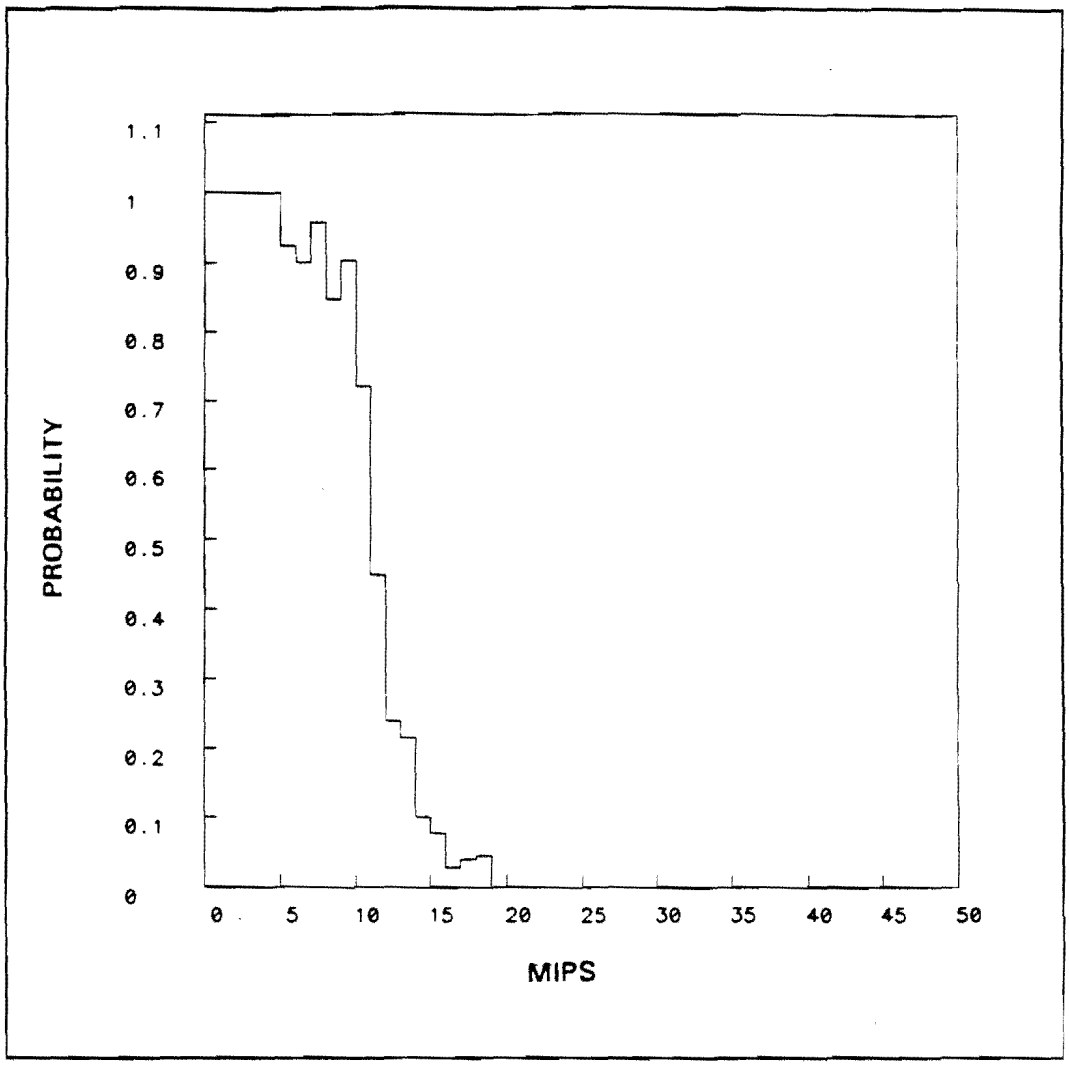

FIGURE 23. Probability of passing the upper level pulse height cut at 13 on wafer 7. To obtain this probability the min(8,9) pulse height is used, where min(8,9) is the pulse height of wafer 8 or wafer 9, whichever is smaller. The probability distribution is the ratio of the min(8,9) pulse height distribution after the cut to that before the cut.

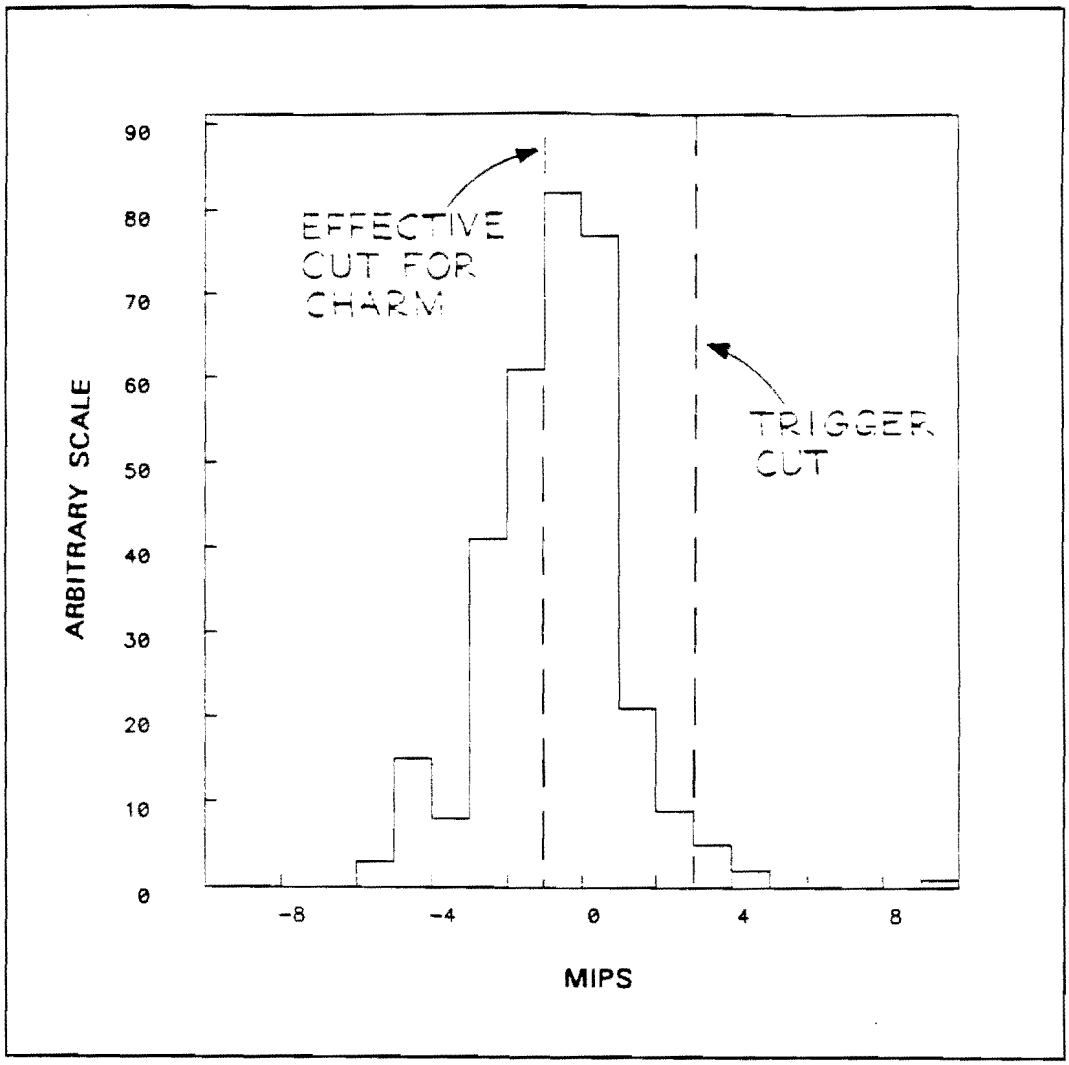

FIGURE 24. The min(8,9) - wafer 7 pulse height difference distribution for a pulse height cut of 13 on wafer 7. Min(8,9) is the pulse height of wafer 8 or wafer 9, whichever is smaller. This distribution is used to predict the probability that a pair of charm particles which decay in the decay region will trigger the apparatus. Background events to the right of the cut at 3 mips will cause a trigger. For a charm event in which each charm particle decays in the decay region to two or more prongs, the distribution would shift to the right by four mips. Thus, in such an event the cut is effectively at -1 mip in the plot above. Data were obtained during the 1985 run of E653.